ChemPlusChem

Research Article
doi.org/10.1002/cplu.202300429

Chemistry Europe
European Chemical Societies Publishing

www.chempluschem.org

Special Collection

Heteronuclear Gold(I)-Copper(I) Complexes with Thia- and Mixed Thia-Aza Macrocyclic Ligands: Synthesis, Structures and Optical Properties

Rocío Donamaría,[a] Vito Lippolis,*[b] José M. López-de-Luzuriaga,*[a] Miguel Monge,[a] and M. Elena Olmos*[a]

The reactivity of the heterometallic polynuclear complexes $[\{Au(R)_2\}_2Cu_2(MeCN)_2]_n$ (R = C_6F_5, C_6Cl_5) with the thioether crowns 1,4,7-trithiacyclononane (**L1**, [12]aneS$_3$), 1,4,8,11-tetrathiacyclododecane (**L2**, [14]aneS$_4$), 1,4,7,10,13,16,19,22-octathiacyclotetracosane (**L3**, [24]aneS$_8$), and the quinoline functionalized pendant arm derivatives of the 12-membered mixed-donor macrocycles 1-aza-,4,7,10-trithiacyclododecane ([12]aneNS$_3$) and 1,7-diaza-4,10-dithiacyclododecane ([12]aneN$_2$S$_2$), **L4** and **L5**, respectively, was investigated in THF solution. While with **L4** and **L5** only ionic compounds of general formulation [Cu(**L**)][Au(R)$_2$] were isolated and structurally characterized (none of them featuring Au···Cu interactions), with **L1**-**L3**, beside similar ionic compounds, some heteronuclear complexes of general formulation [{Au(R)$_2$}{Cu(**L**)}] and featuring Au···Cu interactions were also obtained. All of them display rather unusual non-classical C–H···Au hydrogen interactions. The complexes display in the solid state different optical properties related to their structures, which have been studied experimentally and theoretically *via* TD-DFT calculations. In particular, all compounds of the type [{Au(R)$_2$}{Cu(**L**)}] featuring Au···Cu metallophilic interactions display luminescence in the solid state both at room temperature (RT) and at 77 K. On the contrary, ionic compounds of general formulation [Cu(**L**)][Au(R)$_2$], except [Cu(**L4**)][Au(C_6F_5)$_2$], are not luminescent.

Introduction

Heteronuclear Au(I)/M complexes [M = closed-shell transition and post-transition metal ions, including Au(I)] featuring Au(I)···M metallophilic interactions, represent an important class of compounds in the realm of supramolecular gold chemistry,[1–30] not only from a theoretical point of view,[31–34] but also for their applications following peculiar optical properties linked to the nature of the Au(I)···M chemical bonding in these systems.[35–46]

Because many factors come into play in determining the luminescence properties of these compounds (generally observed in the solid state) including their nuclearity and dimensionality, nature and structural arrangements of the closed-shell metal ions, strength and disposition of the metallophilic interactions, to date it is still a challenging task to draw structure-property relationships for a targeted construction *via* self-assembly of new structural archetypes of controlled nuclearity and dimensionality and desired optical properties for potential applications.

In the last decade, following our interest in the preparation of organometallic gold(I) complexes featuring metallophilic interactions, we have considered for the first time thioether crowns[33,34,47–49] and mixed donor macrocyclic ligands (and their pendant arm derivatives)[50–54] of different ring sizes and number of donor atoms to support Au(I)···M [M = Ag(I), Tl(I)] interactions and fine tune the structural and photophysical properties of the resulting heteronuclear complexes.

In particular, for comparison reasons, a common acid-base synthetic strategy[33,34,47–54] and experimental conditions were adopted, which consist in the reaction of polymeric organometallic Au(I) complexes $[\{Au(C_6X_5)_2M\}]_n$ [M = Ag(I), Tl(I); X = Cl, F] with the chosen organic ligand in low polar solvents (toluene, THF), in different molar ratios depending on the number of donor atoms in the macrocyclic ligand. Following this approach, we have prepared with ligands such as **L1**–**L5** (Scheme 1) compounds of unprecedented structural archetypes and peculiar optical properties *via* formation of M–S/N [M = Ag(I), Tl(I)] and both Au(I)···M and Au(I)···Au(I) unsupported interactions demonstrating the great versatility of these kind of ligands.[33,34,47–54]

For example, an unprecedented *pseudo*-linear M–Au(I)–Au(I)–M disposition of four interacting closed-shell metal ions was observed in the discrete tetranuclear complexes [{Au(C_6F_5)$_2$}

[a] Dr. R. Donamaría, Prof. J. M. López-de-Luzuriaga, Prof. M. Monge, Prof. M. E. Olmos
Departamento de Química, Instituto de Investigación en Química (IQUR), Complejo Científico Tecnológico,
Universidad de La Rioja
Madre de Dios 53, 26004 Logroño (Spain)
E-mail: josemaria.lopez@unirioja.es
m-elena.olmos@unirioja.es

[b] Prof. V. Lippolis
Dipartimento di Scienze Chimiche e Geologiche
Università degli Studi di Cagliari
S.S. 554 Bivio per Sestu, 09042 Monserrato (CA) (Italy)
E-mail: lippolis@unica.it

Supporting information for this article is available on the WWW under https://doi.org/10.1002/cplu.202300429

Part of a Special Collection on Gold Chemistry

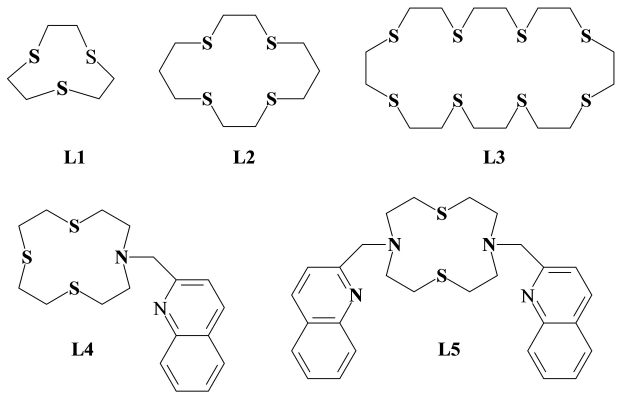

Scheme 1. Macrocyclic ligands considered in this work.

$M(\mathbf{L1})_n]_2$ [n = 2 and 1 for M = Ag(I),[47] Tl(I),[48] respectively], while the complex [{$Au(C_6Cl_5)_2$}Ag(**L2**)] represented the first example of a dinuclear Au(I)/Ag(I) compound featuring an unsupported Au(I)···Ag(I) contact.[47] On passing to the mixed donor macrocycles [12]aneNS$_3$ (1-aza-4,7,10-trithiacyclododecane), [12]aneN$_2$S$_2$ (1,7-diaza-4,10-dithiacyclododecane), and [12]aneNS$_2$O (1-aza-4,10-dithia-7-oxacyclododecane), the complex cations [{$Au(C_6Cl_5)_2$}{Tl(**L**)}$_2$]$^+$ (**L** = [12]aneNS$_3$, [12]aneN$_2$S$_2$) displayed the unprecedented Tl(I)–Au(I)–Tl(I) trinuclear discrete framework,[50] while the neutral binuclear complex [{$Au(C_6Cl_5)_2$}{Ag([12]aneNS$_2$O)}] showed mechanochromism by changing its luminescence upon grinding at room temperature.[52] The use of quinoline functionalized pendant arm derivatives of the mentioned mixed donor tetradentate macrocyclic ligands, such as **L4** and **L5** (Scheme 1), allowed the preparation of polynuclear complexes, featuring optical properties closely related to their structures and nuclearity,[51,53, 54] among which a polynuclear system including for the first time an heterotrimetallic M–Au(I)–M′ moiety [M = Ag(I), M′ = Tl(I)].[53]

Continuing our research program to consider macrocyclic ligands for the preparation of luminescent heteronuclear Au(I)/M [M = closed-shell metal ions] complexes based on metallophilic interactions with structural and optical properties finely tuned by the coordination properties of these kind of ligands,[33,34, 47–55] we report herein the results obtained by reacting the heterometallic starting compounds [{Au-$(C_6X_5)_2$}$_2$$Cu_2$(MeCN)$_2$]$_n$ (X = F, Cl)[56,57] with **L1**–**L5** (Scheme 1) for the formation of Au(I)/Cu(I) heteronuclear compounds. In particular, and in comparison with the results achieved considering Ag(I) and Tl(I) as closed-shell metal ions, we wanted to explore the effect of a different d^{10} transition metal ion, keeping the synthetic strategy the same and considering a group of macrocyclic ligands already studied in the formation of Au(I)/Ag(I) and Au(I)/Tl(I) heteronuclear complexes.

Results and Discussion

Synthesis and characterization

The experimental conditions used for the reactions between [{$Au(C_6X_5)_2$}$_2$$Cu_2$(MeCN)$_2$]$_n$ (X = F, Cl)[56,57] and the ligands **L1**–**L5** are summarized in Scheme 2. In particular, a 1:1 **L**/Cu molar ratio was considered in all cases, except for **L3**, which is able to host two metal centres in its cavity (the use of 1:2 and 1:3 **L**/Cu molar ratios in the case of **L4** and **L5** did always afford compounds featuring a 1:1 **L**/Cu stoichiometry, leaving excess of [{$Au(C_6X_5)_2$}$_2$$Cu_2$(MeCN)$_2$]$_n$ (X = F, Cl) unreacted). The reactions were conducted in THF at room temperature and afforded the complexes **1**–**10**, having the formulation as reported in Scheme 2, after precipitation from the reaction mixture by the addition of *n*-hexane.

Compounds **1**–**10** are solid at room temperature, stable to air and moisture for a long period of time, insoluble in halogenated solvents, *n*-hexane and Et_2O, but they are reasonably soluble in THF and acetone.

The IR spectra of **1**–**10** display, among others, the bands characteristic of the perhalophenyl groups $C_6X_5^-$ (X = F, Cl) bonded to the Au(I) centre (see the Experimental Section). Bands due to the methylquinoline pendant arm(s) are also present in the IR spectra of complexes **7**–**10** in the range 1560–1740 cm^{-1}.

The molar conductivity (Λ_M) measured in acetone solutions (5×10^{-4} M) shows values in the range 105–138 $\Omega^{-1}cm^2mol^{-1}$ for all compounds, but **3** and **6**, typical for 1:1 electrolytes, and in agreement with a ionic formulation [$Au(C_6X_5)_2$]$^-$/[Cu(**L**)]$^+$ (X = F, Cl; **L** = **L1**, **L2**, **L4**, **L5**). For compounds **3** and **6**, Λ_M values of 172 and 199 $\Omega^{-1}cm^2mol^{-1}$, respectively, were measured as expected for 1:2 electrolytes. These data indicate the rupture of the Au(I)···Cu(I) interactions in solution (**1**, **4**, **5**) or the ionic nature of the complexes (**2**, **3**, **7**–**10**).

^{1}H-NMR and ^{19}F-NMR (compounds **1**–**3**, **7**, **8**) spectra were recorded in THF-[D_8] for compounds **1**–**6**, and in acetone-[D_6] for compounds **7**–**10**. The compounds **1**, **4** and **3**, **6** present only one signal as singlet in their ^{1}H-NMR spectrum at 2.93 (**1**), 2.88 (**4**), 3.07 (**3**), and 2.82 ppm (**6**), corresponding to 12 (**1**, **4**) and 32 (**3**, **6**) equivalent methylenic hydrogens. These signals

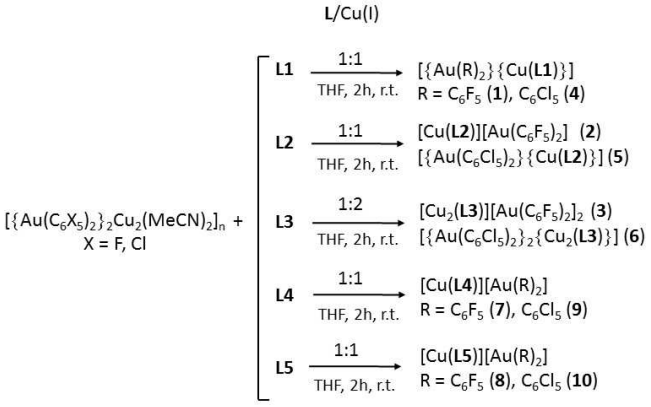

Scheme 2. Synthesis of complexes **1**–**10**.

are slightly shifted with respect to the singlet signals recorded in THF-[D_8] at 3.20 (**L1**) and 2.92 ppm (**L3**) for the uncoordinated macrocyclic ligands, in agreement with Cu(I) coordination to **L1** and **L3** in solution. For compounds **2** and **5**, three sets of signals were observed in their ^{1}H-NMR spectrum at 2.01 (**2**), 1.93 (**5**) (quintet, 4H, S–CH_2–CH_2–CH_2–S), 2.73 (**2**), 2.64 (**5**) (t, 8H, S–CH_2–CH_2–CH_2–S), and 2.85 (**2**), 2.76 (**5**) ppm (s, 8H, S–CH_2–CH_2–S) as compared to the corresponding signals for uncoordinated **L2** recorded at 2.01, 2.74, 2.86 ppm, respectively, in THF-[D_8]. The ^{1}H-NMR spectra of compounds **7**–**10** in acetone-[D_6] show broadened and slightly shifted signals as compared to the corresponding ones observed for the uncoordinated ligands **L4** and **L5**. The signals of the protons belonging to the macrocyclic moieties appear as multiplets at about 3 ppm, while those of the quinoline unit(s) appear as well-defined resonances in the range 7.62-8.57 ppm. The singlet for the protons of the methylenic group bridging the quinoline unit(s) to the macrocyclic frameworks appears at 4.17 (**7**), 4.16 (**9**), and 4.27 (**8**, **10**) ppm as compared to the corresponding signals recorded at 3.95 and 3.94 ppm for uncoordinated **L4** and **L5**, respectively, in the same solvent. On the other hand, the ^{19}F-NMR spectra of **1**–**3** (THF-[D_8]) and **7**, **8** (acetone-[D_6]) present the characteristic pattern in the range −115−−167 ppm typical of the group $[Au(C_6F_5)_2]^-$.

Finally, the MALDI(−) mass spectra of the new compounds show the peak corresponding to the anions $[Au(C_6X_5)_2]^-$ at *m/z* = 531 (X = F, **1**–**3**, **7**, **8**) and *m/z* = 695 (X = Cl, **4**–**6**, **9**, **10**). On the other hand, in the MALDI(+) mass spectra, peaks due to the fragments $[Cu(\mathbf{L})]^+$ appear at *m/z* = 243 (**L1**: **1**, **4**), 331 (**L2**: **2**, **5**), 543 (**L3**: **3**, **6**), 427 (**L4**: **7**, **9**), and 551 (**L**: **8**, **10**), supporting the coordination of Cu(I) to the macrocyclic ligands.

Crystal Structures. The X-ray crystal structures of compounds **1**–**5** and **7**–**10** were established by X-ray diffraction analysis of single crystals grown by diffusion of *n*-hexane into THF solutions of the complexes [see Table S1 in the Supporting Information (SI) for crystallographic details]. In the case of **6**, we were unable to grow single crystals suitable for single-crystal X-ray diffraction studies, while **8** crystallizes with half a molecule of *n*-hexane per molecule of complex.

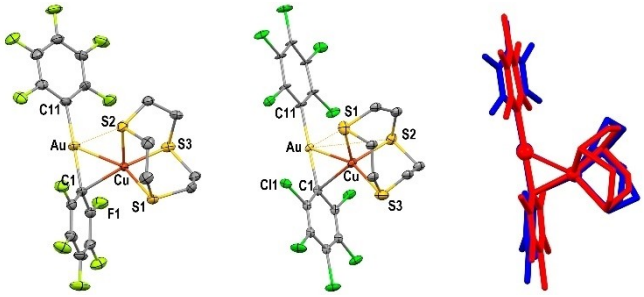

Figure 1. Molecular structures of compounds **1** (left) and **4** (middle) with the labelling scheme adopted. Thermal ellipsoids are drawn at the 50% probability level. Hydrogen atoms have been omitted for clarity. On the right, superimposition of the molecular structures of **1** (blue) and **4** (red).

Both **1** and **4** are discrete dinuclear Au(I)/Cu(I) complexes featuring a $[Au(C_6X_5)_2]^-$ unit [X = F (**1**), Cl (**4**)] linked to the Cu(I) atom of a $[Cu(\mathbf{L1})]^+$ cationic fragment *via* Au···Cu metallophilic interactions of 2.6523(8) and 2.612(3) Å, respectively (Figure 1 and Table 1). The two structures are very similar despite the different halogen atom in the $[Au(C_6X_5)_2]^-$ unit (Figure 1).

In both complexes, the Cu(I) metal centre is involved in a Cu···C interaction with the *ipso* carbon atom of one of the two perhalophenyl rings coordinating the Au(I) atom [Cu···C_{ipso} = 2.259(7) (**1**), 2.30(2) Å (**4**)]. Both Au···Cu and Cu···C_{ipso} distances fall in the ranges observed in heteronuclear Au(I)/Cu(I) systems reported in the literature [Au···Cu = 2.5741(6)–2.9335(11), Cu···C_{ipso} = 2.141(4)–2.919(1) Å].[5,56, 58] (a detailed discussion on the nature of Au···Cu and Cu···C_{ipso} interactions in similar complexes is reported in refs. [59, 60]). Additionally, the cation-anion connection is in both cases reinforced by the presence of weak Au···S interactions of 3.667(2) Å in **1** and of 3.748(12) and 3.818(7) Å in **4**. The Cu(I) metal centres complete to five their coordination number by coordinating the three S-donor atoms from the terminal ligand **L1**, which adopts an endodentate conformation in both structures. Of note, the coordination environment of the Cu(I) centre in **1** and **4** can be described either as distorted square-based pyramid or as distorted trigonal bipyramid due to the fact that the τ parameter considered to discriminate between the two geometries is

Table 1. Main bond or contact distances (Å) and C–H–Au angles (°) in the crystal structures of **1**–**5**.

	1	2	3	4	5
Au···Au	>6	3.7916(1)	>6.5	>8.5	>8
Au···Cu	2.6523(8)	>6.5	>5.5	2.612(3)	2.679(2)
Cu···C_{ipso}	2.259(7)	–	–	2.30(2)	>3
Au–C	2.034(6) 2.068(6)	2.040(4) 2.044(4)	2.048(5)–2.060(5)	2.04(3) 2.05(3)	2.020(11)
Cu–S	2.331(2) 2.372(2) 2.392(2)	2.2776(12)–2.2876(11)	2.2631(13)–2.3658(14)	2.318(8) 2.355(10) 2.399(13)	2.231(3) 2.270(3) 2.400(4)
H···Au	3.095	2.917 3.025	2.875 2.964	2.929	3.254
C(H)···Au	3.870(7)	3.850(5) 3.687(4)	3.601(5) 3.667(5)	3.67(2)	4.217(14)
C–H–Au	137.7	157.6 125.4	132.0 132.1	127.5	164.5
Ct···Ct[a]	–	3.754	3.940 3.520	–	–

[a] Centroid(Ct)-Centroid(Ct) distances between perhalophenyl rings involved in π-π interactions.

approximately 0.5 in both compounds [0.54 (**1**), 0.53(**4**)].[61] Interestingly, this is the first time this coordination geometry is observed in Cu(I) complexes with **L1**. In the previous reported complexes [Cu(**L1**)]I, $[Cu_2(\mathbf{L1})_3](BF_4)_2$, and [{Cu(**L1**)}{$As(PPh_3)$}]$ClO_4$ a tetrahedral coordination environment has been observed around Cu(I), due to a coordination number of four around the copper(I) metal centre.[62–64] The Cu–S bond distances range between 2.318(8) and 2.399(13) Å, and lie within the range of Cu–S distances described for other Cu(I) complexes with **L1** [2.238(1)–2.424(6) Å].[62–64] It is worth to recall that starting from $[\{Au(C_6F_5)_2M]_n$ [M = Ag(I), Tl(I)] the tetranuclear complexes [{$Au(C_6F_5)_2$}{$Ag(\mathbf{L1})_2$}]$_2$ and [{$Au(C_6F_5)_2$}{Tl(**L1**)}]$_2$ were obtained and structurally characterized, which feature almost linear $(\mathbf{L1})_2$Ag–Au–Au–Ag$(\mathbf{L1})_2$ and (**L1**)Tl–Au–Au–Tl(**L1**) arrangements, respectively, held together by unsupported metallophilic and aurophilic interactions.[47,48] Starting from $[\{Au(C_6Cl_5)_2\}M]_n$ [M = Ag(I), Tl(I)], microcrystalline compounds of analogous stoichiometry were isolated.[47,48]

It is worth noting that the crystal structures of **1** and **4** display unusual non-classical C–H···Au hydrogen interactions with H–Au distances of 3.095 and 2.929 Å, respectively, as well as F···F (2.858 and 2.886 Å) in **1** or Cl···Cl contacts in **4** (3.447 and 3.458 Å), which give rise to extended sheets normal to the crystallographic *z* axis (Figure S1 in the SI).

Compounds **2** and **5** obtained from the reaction of **L2** with $[\{Au(C_6X_5)_2\}_2Cu_2(MeCN)_2]_n$ [X = F(**2**), Cl(**5**)] present a different structure depending on the nature of the halogen atom on the perhalophenyl rings coordinating the Au(I) atom. In fact, complex **2** is ionic and features in the asymmetric unit a $[Cu(\mathbf{L2})]^+$ complex cation balanced by the anion $[Au(C_6F_5)_2]^-$; no metallophilic interactions between the two complex ions are present (shortest Au–Cu distance > 6.5 Å). In $[Cu(\mathbf{L2})]^+$, the Cu(I) centre sits inside the cavity of **L2**, which provides a distorted tetrahedral array of sulphur atoms with Cu–S bond distances and S–Cu–S bond angles in the ranges 2.2776(12)–2.2876(11) Å and 94.53(4)–126.42(4)°, respectively (Figure S2 in the SI). This result is quite interesting in connection with the presumed inability of **L2** to distort sufficiently to attain a tetrahedral geometry for a metal ion guest. This hypothesis was put forward to justify both the coplanar arrangement of Cu(II) with the four S-donors in $[Cu(\mathbf{L2})](ClO_4)_2$ [Cu–S = 2.308(1), 2.297(1), S–Cu–S = 89.9(4), 90.1(4)],[65] and the polymeric structure observed in {[Cu(**L2**)]ClO_4}$_n$, in which a distorted tetrahedral geometry around each Cu(I) is achieved *via* three S-donor atoms from a coordinated ligand unit and one S-donor atom from an adjacent $[Cu(\mathbf{L2})]^+$ cation [Cu–S = 2.260(3)–2.342(3) Å, S–Cu–S = 88.8–113.0°].[66]

Complex **5** is a dinuclear Au(I)/Cu(I) compound sitting on a two-fold screw axis and featuring a linear $[Au(C_6Cl_5)_2]^-$ fragment linked to the copper(I) atom of the $[Cu(\mathbf{L2})]^+$ cation *via* an unsupported Au···Cu interaction of 2.679(2) Å, although in this case, in contrast with what is found in the structures of **1** and **4**, no Cu···C_{ipso} interaction is observed (Figure 2 and Table 1).

The copper(I) centre completes a tetrahedral coordination sphere *via* three S-donor atoms from the macrocyclic ligand [Cu–S = 2.231(3)–2.400(4) Å], the fourth S-donor atom being at 3.352(5) Å distance from Cu(I). In the analogous [{$Au(C_6Cl_5)_2$}Ag(**L2**)] dinuclear complex, all four S-donor atoms from the **L2** are coordinated to the Ag(I) centre.[47] The copper(I) centre in **5** is disordered over two sites with statistically the same occupancy of 50%. The two components of the disorder model differ for the uncoordinated S-donor atom (Figure 2), being either S1 or $S1^{\#1}$ (#1 = −x + 1, y, −z + 3/2). The reason why the $[Au(C_6F_5)_2]^-$ anion does not interact with the $[Cu(\mathbf{L2})]^+$ complex cation *via* metallophilic interaction in compound **2** might be the higher electronegativity of the fluorine atoms, which render the $[Au(C_6F_5)_2]^-$ anion less basic than $[Au(C_6Cl_5)_2]^-$. This hypothesis is supported by the X-ray crystal structure of compound **3** and by the optical properties of compound **6** (see below). However, the presence of Au···Cu interactions in both **1** and **4** suggests that also the coordination properties and stereochemical demands of the macrocyclic ligands might have an influence.

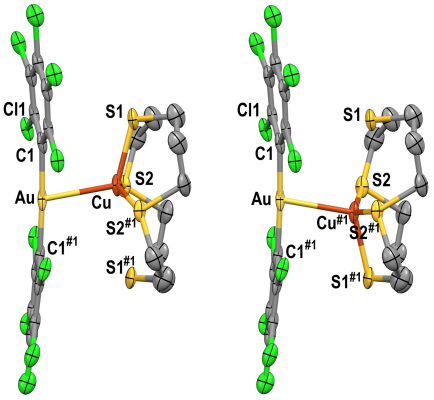

Figure 2. Molecular structure of compounds **5** with the labelling scheme adopted (the two components of the disorder model are shown). Thermal ellipsoids are drawn at the 30% probability level. Hydrogen atoms have been omitted for clarity. Symmetry operation: #1 = −x + 1, y, −z + 3/2.

Similarly to what is observed in **1** and **4**, complexes **2** and **5** also display C–H···Au hydrogen interactions as well as other weak interactions, although in these cases the expansion of the structures *via* non-covalent interactions differs depending on the halogen present in the complex. Thus, while the crystal packing in **2** results in polymeric chains formed through C–H···Au hydrogen interactions, π-π and very weak Au···Au interactions between two adjacent $[Au(C_6F_5)_2]^-$ units (according to the recent values published for the van der Waals radius of gold varying from 2.14[67] to 2.32[68] or even 2.45 Å[69]) (Figure S3 in SI and Table 1), a two-dimensional network similar to those commented above for **1** and **4** is observed for **5** (Figure S4 in SI and Table 1). The H···Au distances in **2** (2.917 and 3.025 Å) are similar to those in **1** and **4**, while in **5** (3.254 Å) they are clearly longer than in the other three structures (see Table 1).

As observed in complex **2**, compound **3** is also ionic, and it features $[Cu_2(\mathbf{L3})]^{2+}$ dinuclear dications lying on crystallographic inversion centres balanced by $[Au(C_6F_5)_2]^-$ anions with no metallophilic interactions among them (Figure S5 left in the SI) (the asymmetric units consists of two half cations and two anions). Each copper(I) centre in $[Cu_2(\mathbf{L3})]^{2+}$ is coordinated to four S-donor atoms in a distorted tetrahedral geometry with

Cu–S bond distances ranging from 2.2631(13) to 2.3658(14) Å, similar to the bond distances observed in $[Cu_2(\mathbf{L3})](BF_4)_2$ and $[Cu_2(\mathbf{L3})](ClO_4)_2$.[70] The shortest Au···Au, Au···Cu and Cu···Cu distances in **3** are 6.952, 5.562 and 4.656 Å, respectively. Interestingly, in $[\{Au(C_6X_5)_2\}_2\{Ag_2(\mathbf{L3})\}]$ (X = F, Cl),[47] $[\{Au(C_6F_5)_2\}_2\{Tl_2(\mathbf{L3})\}]$, and $[\{Au(C_6Cl_5)_2\}_2\{Tl_2(\mathbf{L3})\}]_n$,[48] both Ag(I) or Tl(I) metal centres coordinated by **L3** in the dinuclear $[M_2(\mathbf{L3})]^{2+}$ units, interact with a $[Au(C_6X_5)_2]^-$ unit *via* metallophilic interactions to afford discrete Au–M–**L3**–M–Au tetranuclear sequencies; in the latter,[48] further aurophilic interactions give rise to –{Au–Tl–**L3**–Tl–Au–Au–Tl–**L3**–Tl–Au}$_n$– polymeric arrays. This different behaviour of Cu(I) with respect Ag(I) and Tl(I) in the formation of heterometallic Au(I)/M(I) complexes with **L1**–**L3** could be determined by the different dimensions of the three d^{10} metal ions, which bring the smaller Cu(I) to satisfy easier/preferably its stereochemical demands with lower coordination numbers.

Again, complex **3** displays C–H···Au hydrogen interactions, with H···Au distances of 2.875 and 2.964 Å (the former being the shortest found in these five crystal structures), and π-π interactions between adjacent $[Au(C_6F_5)_2]^-$ units (distances between centroids of 3.940 and 3.520 Å), which, together with additional C–H···F hydrogen bonds, result in a 3D network (Figure S5 right in SI and Table 1).

As in the case of **2** and **3**, no metallophilic interactions are observed in the crystal structures of compounds **7**, **9** and **8**·0.5*n*-hexane, **10** obtained from the reaction of $[\{Au(C_6X_5)_2\}_2Cu_2(MeCN)_2]_n$ with **L4** and **L5**, respectively (see Scheme 2).

All four complexes are ionic and feature $[Cu(\mathbf{L})]^+$ and $[Au(C_6X_5)_2]^-$ units [**L** = **L4**, X = F (**7**), Cl (**9**); **L** = **L5**, X = F (**8**·0.5*n*-hexane), Cl (**10**)], which are only connected through C–H···Au hydrogen interactions, which are also present in these four structures and that display H–Au distances ranging from 2.821 to 3.221 Å (see Table 2, Figure 3 for **7**, and Figure S6 in the SI for **8**·0.5*n*-hexane **9**, and **10**).

Depending on the number of the quinoline functionalized pendant arms in the two ligands, the coordination environment around copper(I) is different. In particular, **L4** binds the Cu(I) metal centre through all five donor atoms imposing a distorted square-based pyramidal geometry (τ = 0.11 and 0.12 for Cu(I) in **7** and **9**, respectively), while a very distorted tetrahedral geometry [S/N–Cu–S/N = 80–130°] is observed in the cases of **8**·0.5*n*-hexane and **10** with **L5** binding the Cu(I) centre *via* one tertiary N-donor (N_{Mc}) and two S-donor atoms from the macrocyclic framework, and the N atom from one quinoline moiety (N_Q). Concerning bond distances, while Cu–N_Q are very similar in the four structures [2.050(4) (**7**), 2.053(3) (**8**·0.5*n*-hexane), 2.010(4) and 2.018(4) (**9**), and 2.038(7) (**10**) Å], the Cu–N_{Mc} bond distances show a higher variability with the shortest ones observed in the complexes with a tetrahedral coordination around Cu(I) [2.305(4) (**7**), 2.181(3) (**8**·0.5*n*-hexane), 2.233(4) and 2.236(4) (**9**), and 2.218(7) (**10**) Å]. The Cu–S bond distances are in general shorter in **8**·0.5*n*-hexane and **10** featuring a distorted tetrahedral coordination at the Cu(I) centre [2.2602(12) and 2.2816(13) Å (**8**·0.5*n*-hexane) and 2.260(3) and 2.276(3) Å (**10**)] than in **7** or **9**, in which the Cu–S distances range between 2.2555(16) and 2.8774(15) Å in **7** and between 2.2354(15) and 2.8409(15) Å in **9**. Interestingly, a similar ionic nature has been observed also for the compounds $[Ag(\mathbf{L})][Au(C_6F_5)_2]$ (**L** = **L4**, **L5**) with the main difference that in the $[Ag(\mathbf{L5})]^+$ cation the ligand binds the metal centre through all six donor atoms imposing a highly distorted octahedral geometry.[54]

The same coordination mode of **L4** and **L5** at Ag(I) is observed in the polynuclear compounds $[\{Au_2Ag_2(C_6F_5)_4\}\{Au(C_6F_5)_2\}_2\{Ag(\mathbf{L4})\}_2]$ and $[\{Au_2Ag_2(C_6F_5)_4\}\{Au(C_6F_5)_2\}\{Ag(\mathbf{L5})\}]_n$ with the difference that in both these compounds the $[Ag(\mathbf{L4})]^+$ and $[Ag(\mathbf{L5})]^+$ cations, respectively, contribute to the formation of

Table 2. Main bond or contact distances (Å) and C–H–Au angles (°) in the crystal structures of **7**–**10**.

	7	**8**·0.5*n*-hexane	**9**[b]	**10**
Au–C	2.049(5) 2.055(5)	2.036(4) 2.039(5)	2.047(5)– 2.054(5)	2.045(9) 2.069(10)
Cu–S	2.2555(16) 2.5517(15) 2.8774(15)	2.2602(12) 2.2816(13)	2.2354(15)– 2.8409(15)	2.260(3) 2.276(3)
Cu–N_{MC}	2.305(4)	2.181(3)	2.233(4) 2.236(4)	2.218(7)
Cu–N_Q	2.050(4)	2.053(3)	2.010(4) 2.018(4)	2.038(7)
H···Au	2.917 2.993 3.137	2.821 3.002 3.221 2.839	2.915– −3.193	2.973 3.029
C(H)···Au	3.770(6) 3.705(6) 3.982(6)	3.739(4) 3.880(4) 4.134(5) 3.591(4)	3.768(6)– −4.156(6)	3.844(11) 3.721(11)
C–H–Au	147.2 134.5 146.5	158.2 150.8 157.2 134.5	135.0– −166.6	150.0 132.2
Ct···Ct[a]	3.596	3.741	3.689	–

[a] Centroid(Ct)-Centroid(Ct) distances between perhalophenyl rings involved in π-π interactions; [b] for **9** a variation range is given for the C–H···Au structural parameters.

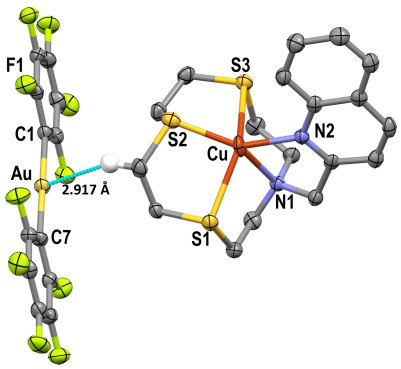

Figure 3. Molecular structures of compound **7** with the labelling scheme Thermal ellipsoids are drawn at the 50% probability level. Hydrogen atoms, except one involved in the C–H···Au hydrogen interaction (white-grey colour), have been omitted for clarity.

$[Au_2Ag_2(C_6F_5)_4]$ tetranuclear units *via* bridging Ag–S bonds.[54] Furthermore, the quinoline functionalized pendant arm derivative of [12]aneNS$_2$O (1-aza-4,10-dithia-7-oxacyclododecane), structurally analogous of **L4**, coordinates Tl(I) with all five donor atoms, and the metal centre completes its coordination sphere though a Au···Tl metallophilic interaction with a $[Au(C_6Cl_5)_2]^-$ unit.[53] In **7**, couples of symmetry-related $[Cu(\mathbf{L4})]^+$ cations are paired along the (100) direction *via* π-π stacking interactions of 3.596 Å (centroid-to-centroid distance) between the quinoline moieties, which together with the previously commented non-classical C–H···Au hydrogen interactions give rise to an extended two-dimensional system (Figure S7), which further result in a 3D network by additional F···F contacts and C–H···F hydrogen bonds. A similar situation is observed in **9**, which features the same cationic $[Cu(\mathbf{L4})]^+$ fragments, which are connected to the aurate(I) anions *via* C–H···Au hydrogen interactions. The difference is that in this case, the $[Au(C_6Cl_5)_2]^-$ units are ordered in a 3D network *via* Cl···Cl contacts ranging from 3.380 to 3.497 Å, and form alternate-fused rectangular- and square-shaped cavities (Figure S8). The former host couples of $[Cu(\mathbf{L4})]^+$ cations coupled *via* π-π interactions of 3.689 Å (centroid-to-centroid distance) between quinoline units, while the latter host couples of non-interacting $[Cu(\mathbf{L4})]^+$ cations facing head-to-tail (Figure S8). Also in compound **8**·0.5*n*-hexane, polyanionic cavities are formed in the crystal packing *via* F···F (2.829 Å) and F···H (2.561 Å) interactions involving $[Au(C_6F_5)_2]^-$ units, and $[Au(C_6F_5)_2]^-$ and *n*-hexane molecules, respectively (Figure S9). Two symmetry-related $[Cu(\mathbf{L5})]^+$ cations interconnected *via* π-π interactions of 3.741 Å between the uncoordinated quinoline moieties sit inside each cavity, and they interact with the polyanionic net through C–H···Au hydrogen interactions (Figure S9). Finally, in compound **10**, square-shaped cavities of interacting $[Au(C_6Cl_5)_2]^-$ units *via* Cl···Cl contacts of 3.445 Å are observed in the crystal packing, which host couples of non-interacting and symmetry-related $[Cu(\mathbf{L5})]^+$ cations, which as the previous cases are connected to the anionic net *via* C–H···Au hydrogen interactions (Figure S10).

Photophysical properties

The absorption spectra of compounds **1**–**6** in diluted THF solutions show similar structural features. In particular, they all present two bands in the ranges 240–243 and 257–260 nm (Table 3), respectively, which are also present in the spectra of the gold(I) precursors $[\{Au(C_6X_5)_2\}_2Cu_2(MeCN)_2]_n$ and $NBu_4[Au(C_6X_5)_2]$ (X = F, Cl), and can be assigned, therefore, to π→π* and Au→π* transitions involving the perhalophenyl groups and the Au(I) metal centres.[45]

The contribution to the band at higher energy of an n→σ* transition within **L1**–**L3**, which falls at 234 nm for the free three thioether ligands, cannot be ruled out (Table 3). **4**–**6** present also a band at 274 nm and a band at 293 (**4**) or 304 nm (**5**, **6**) that may still concern the perchlorophenyl groups. Interestingly, compounds **1** and **4**, both featuring **L1** as macrocyclic ligand, also show a weak band at 320 and 366 nm, respectively, similar to those observed for $[\{Au(C_6X_5)_2\}_2Cu_2(MeCN)_2]_n$ (X = F, Cl), which could indicate the presence to some extent of a Au···Cu interaction also in solution for these complexes. The absorption spectra in the solid state of **1**–**6** are characterized by a band at high energy with two maxima at 245 and 265 nm for **1**–**3** and 240 and 280 nm for **4**–**6**. In the absorption spectra of **1** and **4**–**6** an additional weak band is observed at 338 and 370 nm, respectively, which is not present in the spectra of both $NBu_4[Au(C_6X_5)_2]$ (X = F, Cl) and complexes **2** and **3**, which do not display metallophilic interactions in the solid state (apart from a very weak aurophilic interaction in **2**).

Therefore, this band could be assigned to an electronic transition that involves the interacting metal centres. By analogy, it can be inferred, therefore, that Au···Cu interactions might be present in the solid state also in compound **6** for which an X-ray diffraction analysis was not possible.

The differences observed between the absorption spectra of **1**, **4**–**6** and those of **2** and **3**, are paralleled by the luminescent properties of these compounds, which points out the relevance of the metallophilic interactions in determining the phopto-physical properties of **1** and **4**–**6**. In fact, as contrary to **2** and **3**,

Table 3. Photophysical properties of complexes **1**–**6**, **7**, **9**.[a]

	Uv-vis (THF) λ/ε/[b]	Solid (RT) $\lambda_{em}/\lambda_{exc}$	Solid (77 K) $\lambda_{em}/\lambda_{exc}$	τ(ns)	Φ(%)
1	243/14245, 260/9217, 320/1599	474, 509(sh)/367	509/347	150.2	26
2	243/14499, 260/8785				
3	243/23873, 260/12322				
4	240/24198, 257/16605, 274/12898, 293/10677, 366/2647	529/425	529/425	726.1	16
5	240/26603, 257/20968, 274/18222, 304/4544	561/408	540/375	154.1	12
6	240/33964, 257/25543, 274/22895, 304/6508	479/358	475/358	194.0	40
7	247/12369, 264/8407, 306/4259, 319/3724	595/366	595/440	739	5.7
9	258/18141, 276/17189, 305/7970, 318/4919	596/367	596/390	871	5.3
L1	234/590				
L2	234/668				
L3	234/2269				
L4	240/1919, 260/1379, 303/1031, 316/1206				

[a] Wavelengths (λ) are given in nm. [b] ε is given in $M^{-1}\,cm^{-1}$.

1 and **4**–**6** display luminescence in the solid state both at room temperature (RT) and at 77 K (Table 3); while in THF solution none of compounds **1**–**6** are emissive, probably due to the rupture of the metal-metal interaction or to a solvent quenching effect. The blue luminescence of **1** at RT is characterized by a $\lambda_{em}=474$ nm with a shoulder at 509 nm ($\lambda_{exc}=367$ nm); only one emission band at 509 nm ($\lambda_{exc}=347$ nm) is observed at 77 K (Figure 4). This might indicate for **1** the presence of two excited states at RT vibrationally interlinked, and that both emissions are obtained with the same excitation energy; at lower temperature, the emission takes place from only one excited state at lower energy.

On the other hand, compound **4** that features structural features very similar to those of **1**, displays a green fluorescence in the solid state with one emissive band at 529 nm ($\lambda_{exc}=$ 425 nm) both at RT and at 77 K (Figure 4). The different halogen atoms in the bis(perhalophenyl)gold(I) units of the two compounds might be responsible of the different emissive properties. Also, as we have commented above, the Au–Cu distances for **1** and **4** are 2.65 and 2.61 Å, respectively. These can influence the observed shift of their emissive properties, by the relationship between a shorter intermetallic distance with a shorter HOMO-LUMO gap.

Compound **5** shows only one emission band at 561 nm ($\lambda_{exc}=408$ nm) at RT that blue-shifts to 540 nm at 77 K (Figure 4). Instead, no dependence from the temperature was observed for the luminescence of compound **6** as only one emission band is observed for this compound in the solid state at 479 nm ($\lambda_{exc}=358$ nm) both at RT and 77 K.

The lifetimes (τ) of emissions of **1** and **4**–**6** at RT are in the range of hundreds of nanoseconds. In particular, for **1**, **5** and **6** τ ranges from 150.2 to 194.0 ns indicating a fluorescent character for the emission transition processes. In the case of **4** a τ value of 726.1 ns was measured, which might indicate a phosphorescent nature for the electronic transition at the base of the luminescent observed in the solid state. The presence of heavy metal centers in the complexes favors the intersystem crossing thanks to the heavy atom effect, leading to emissions from the triplet state and, therefore, long lifetimes in some complexes.

Despite compounds **7**–**10** feature the absence of Au···Cu interactions in their structures, those obtained from **L4** display luminescence in the solid state, and therefore, we studied their optical properties more in detail. Presumably, **8**·0.5*n*-hexane and **10** are not luminescent in the solid state due to a quenching effect of the uncoordinated quinoline moiety of **L5** (see above).

The Uv-vis absorption spectra of **7** and **9** in THF solutions show two bands at high energy at 247/264 nm for **7**, and 258/276 for **9** (Table 3), which can be tentatively assigned to transitions involving either the perhalophenyl groups of the $[Au(C_6X_5)_2]^-$[45] units or the macrocyclic ligand (see Table 3 for the absorption bands recorded for **L4** as free ligand in THF solution). On the other hand, the bands observed at lower energy at 306/319 nm for **7**, and 305/318 nm for **9**, can be assigned to electronic transitions within the quinoline moiety of coordinated **L4**. As mentioned, **7** and **9** display similar luminescence properties in the solid state with an emission maximum at 595 and 596 nm, respectively, that doesn't shift on passing from RT to 77 K (Figure 5).

The lifetimes of emissions of **7** and **9** (730 and 871, respectively) and the low quantum yields (5.7 and 5.3%, respectively) suggest the emissions could be determined by phosphorescence processes in both compounds.

Theoretical calculations

In order to find out the origin of the luminescence properties of the compounds discussed above on the basis of their structural features, single-point DFT calculations were performed on model systems **1a**, **4a**, and **5a** built from the solid-state structures of complexes **1**, **4**, and **5**. Model **7a** representing the complex cation $[Cu(\mathbf{L4})]^+$ in both **7** and **9** was first optimized at DFT level (Figure 6). Considering the similarity of the optical properties of **7** and **9**, despite the different anionic moieties in the two compounds, we thought the origin of their luminescence could be determined only by the $[Cu(\mathbf{L4})]^+$ unit. In order to provide support to the behavior in solution of complexes displaying intermetallic interactions we fully optimized complex **1** in the gas phase (model **1b**) and using implicit solvent through the SMD model (model **1c**) (see Table S2 in SI). The

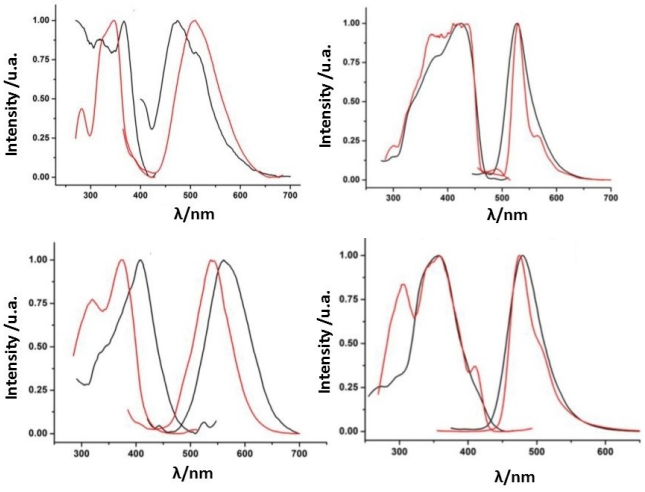

Figure 4. Excitation and emission spectra of **1** (up-left), **4** (up-right), **5** (down-left), and **6** (down-right) in the solid state at RT (black line) and 77 K (red line).

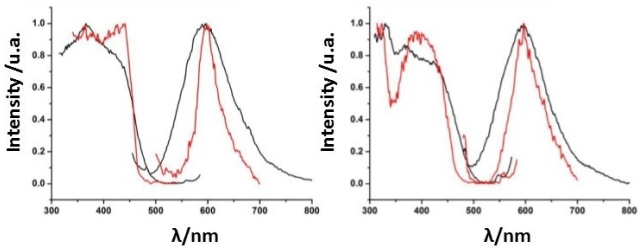

Figure 5. Excitation and emission spectra of **7** (left), **9** (right), in the solid state at RT (black line) and 77 K (red line).

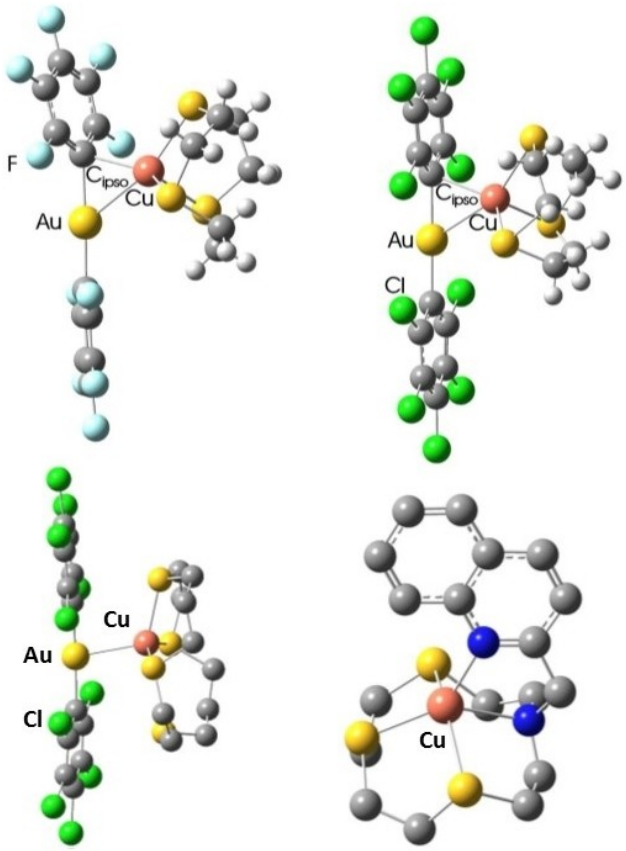

Figure 6. Theoretical model systems considered for TD-DFT calculations [{Au(C_6F_5)$_2$}{Cu(**L1**)}] (**1a**, up-left), [{Au(C_6Cl_5)$_2$}{Cu(**L1**)}] (**4a**, up-right), [{Au(C_6Cl_5)$_2$}{Cu(**L2**)}] (**5a**, down-left), [Cu(**L4**)]$^+$ (**7a**, down-right).

results show that the optimization of **1b** in the gas phase shows very similar Au–Cu and C_{ipso}–Cu distances to those observed experimentally, whereas the full optimization of model **1c**, using implicit solvent, leads to a slight increase of these interaction distances, what would be related to the proposed interaction rupture when explicit donor solvent is present.

To describe the non-covalent interactions responsible for the stabilization of the complexes we computed the non-covalent interactions (NCI) isosurfaces for the emissive complexes **1**, **4**, **5** and **7** (see Computational details and Figure S11 in SI). As it can be observed, compounds **1**, **4** and **5** display strong non-covalent Au···Cu interactions (blue isosurface) that are supported by a covalent 3-center 2-electron Au–C_{ipso}–Cu bond for complex **1**, a strong Cu–C_{ipso} interaction (blue isosurface) in the case of complex **4** and a weak van der Waals C_{ipso}–S in the case of complex **5**. The NCI calculations on complex **7** shows a C–H···Au bonding interaction that links the anionic and cationic parts in the solid state. The NCI results agree with the previously reported ab initio analysis of the Au(I)···Cu(I) interaction in acid-base bis(perhalophenyl)aurate-copper(I) systems for which strong interactions of more than 500 kJ·mol^{-1} were described. These interactions have an ionic nature (more than 80% already observed at Hartree-Fock level of theory), reinforced a by dispersive component of *ca.* 20% contribution to the total metallophilic interaction energy. In addition, the Cu(I)···C_{ipso} interactions studied for these Au(I)–Cu(I) systems provided an additional stabilization of *ca.* 70 kJ·mol^{-1} of dispersive nature.[59,60]

The electronic structure of the model systems considered was first computed to analyse the contribution of each of their parts to the frontier molecular orbitals (MOs) involved in the electronic transitions responsible of the optical properties observed. The results for **1a**, **4a**, and **5a**, will be analysed first.

In the case of **1a** (see Table S3 for the population analysis and Figure S12 for frontier MOs) the highest occupied MO (HOMO) is mainly located on the [Cu(**L1**)]$^+$ moiety [61%, with a high participation (39%) of the Cu(I) metal centre]. The same features are observed for HOMO-6 with an even higher contribution from Cu(I) (54%). On the contrary, the HOMO-4 orbital is mainly located on the anionic fragment [Au(C_6F_5)$_2$]$^-$ with a participation of 49% of the gold(I) atom. On the other hand, the lowest unoccupied MO (LUMO) is mainly centred on the anionic part of the molecule (76%) with a contribution of 61% from one C_6F_5 ligand and 15% from Au(I). The orbitals LUMO+1 and LUMO+4 are mainly located on the [Cu(**L1**)]$^+$ cation (80 and 79%, respectively).

In the case of model **4a** (Table S3, Figure S13), the HOMO is equally (50%) located on the two fragments [Cu(**L1**)]$^+$ and [Au(C_6Cl_5)$_2$]$^-$, while HOMO-1, HOMO-4, HOMO-5 and HOMO-7 are mainly centred on the anionic part of the molecule (94, 84, 95, and 68%, respectively). The orbital HOMO-3 is mainly localized on the cationic part of the molecules with an elevate contribution (47%) from Cu(I). For LUMO the main contribution (76%) arises from the C_6Cl_5 ligands, while the whole molecule participates to LUMO+1 (55% for [Cu(**L1**)]$^+$ and 46% for [Au(C_6Cl_5)$_2$]$^-$).

For the model system **5a**, the HOMO is mainly located on the [Cu(**L2**)]$^+$ moiety (89%), while the LUMO is centred mainly on the [Au(C_6Cl_5)$_2$]$^-$ anionic fragment (74%) with a significant participation of the Cu(I) centre (22%). The HOMO-1 is practically located on the entire [Au(C_6Cl_5)$_2$]$^-$ fragment with a major contribution from the C_6Cl_5 ligands (Table S4, Figure S14).

The first singlet-singlet excitation energies where computed for **1a**, **4a**, and **5a** at the TD-DFT level of theory (see Experimental Section). Since the lifetime for **4** is near the microseconds range, the lowest singlet-triplet excitation was also computed for **4a**. In this way, considering the character of the MOs involved, it was possible to elucidate the nature of the computed electronic transitions and to compare them with the experimental Uv-vis absorption spectra.

The most intense singlet-singlet excitations for **1a** (Table S5) are calculated in the range between 293.3 and 242.6 nm (being these two the most intense), in agreement with the experimental absorption spectrum recorded in the solid state (Figure 7). The former mainly consists of a HOMO→LUMO transition corresponding to a charge-transfer from the [Cu(**L1**)]$^+$ moiety to the [Au(C_6F_5)$_2$]$^-$ fragment (see Table S3). The excitation calculated at 242.6 nm consists of a mixture of the transitions HOMO-6→LUMO, HOMO-4→LUMO, and HOMO→LUMO+4, which correspond overall to a charge-transfer between the

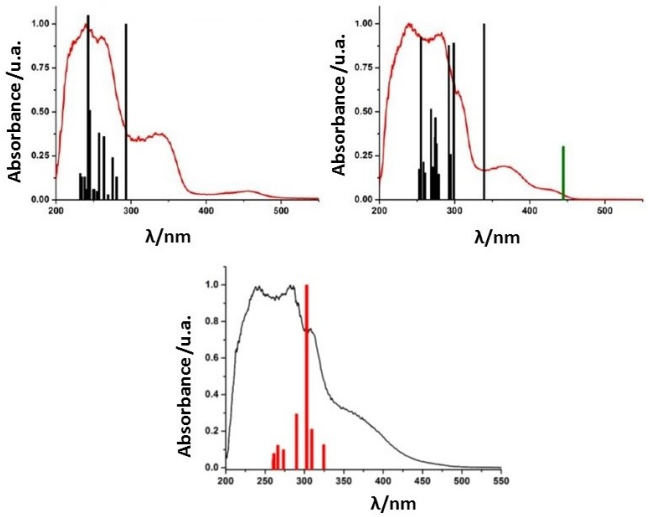

Figure 7. Experimental Uv-vis solid state absorption spectrum (red line) and TD-DFT singlet-singlet calculated excitations (black bars) for model systems **1a** (up-left), **4a** (up-right), and **5a** (down). The lowest singlet-triplet (green bar) excitation for model **4a** is also included (the green bar only represents the energy of the computed singlet-triplet transition, since the oscillator strength cannot be estimated).

complex cation and the aurate(I) fragments with a contribution from transitions internal to the two moieties.

Similar results were obtained for **4a**. The most intense singlet-singlet calculated excitations appear in the range 339.1–253.3 nm in agreement with the band at higher energy observed in the experimental Uv-vis spectrum recorded in the solid state (Figure 7).

Analogously to **1a**, the most intense excitation at 339.1 nm calculated for **4a** arises from the HOMO→LUMO transition, which corresponds to a charge-transfer from the $[Cu(\mathbf{L1})]^+$ moiety to the $[Au(C_6Cl_5)_2]^-$ fragment (Table S3). The rest of the calculated singlet-singlet transitions for **4a** consist of an admixture of transitions (Table S3) that in part imply charge-transfers between the two ionic fragments forming the compound, and for the rest imply charge-transfers within each of them. The singlet-triplet excitation is calculated an at 444.8 nm and corresponds to an HOMO→LUMO transition as calculated for the singlet-singlet transition of the highest intensity.

Similar considerations apply to the model system **5a** for which the most intense singlet-singlet calculated excitations are reported in Table S6 and their superimposition to the experimental Uv-vis spectrum recorded in the solid state is shown in Figure 7.

The hypothesis the similar luminescence properties of **7** and **9** could be determined by the common cation fragment $[Cu(\mathbf{L4})]^+$ rather than by the different anionic ones $[Au(C_6X_5)_2]^-$ (X = F (**7**), Cl (**9**)], brought us to perform theoretical calculations on model **7a** to explain the optical properties of the two compounds. The model **7a** optimized at DFT level showed calculated structural features very similar to those observed in the solid state for $[Cu(\mathbf{L4})]^+$ in **7** and **9**, which are almost superimposable (Figure S15). A study of the frontier MOs (Figure 8) for model **7a** along with a population analysis (Table S7) was first undertaken.

While the unoccupied orbitals LUMO and LUMO + 1 are localized on the methyl-quinoline moiety of **L4** (98%, see Figure 8 and Table S7), LUMO + 2 is mainly located on the macrocyclic portion of **L4** (81%), and LUMO + 3 is located both on this same portion of the ligand (42%) and on the Cu(I) metal centre (58%). On the other hand, the occupied MOs HOMO-HOMO-3, and HOMO-7 are mainly located on the macrocyclic moiety of the ligand and on the copper(I) atom (67–99%). However, HOMO-4 is distributed all over the $[Cu(\mathbf{L4})]^+$ cation, and HOMO-6 is located mainly on the methyl-quinoline fragment. The most intense singlet-singlet excitations for **7a** were calculated in the range 306.5–237.6 nm (Table S8) and well agree with the absorption bands at higher energy recorded for **7** and **9** in the solid state (Figure 9).

The most intense calculated excitation at 306.5 nm consists of an electronic transition from the HOMO-2 to the LUMO, which can be described as a charge-transfer from the macrocyclic moiety of the ligand and the copper(I) centre to the methyl-quinoline fragment. The analysis of the rest of the calculated singlet-singlet transitions indicates for them a charge-transfer nature either between the different parts of the $[Cu(\mathbf{L4})]^+$ cation or internal each of these parts (macrocyclic and quinoline fragments, and copper(I) atoms).

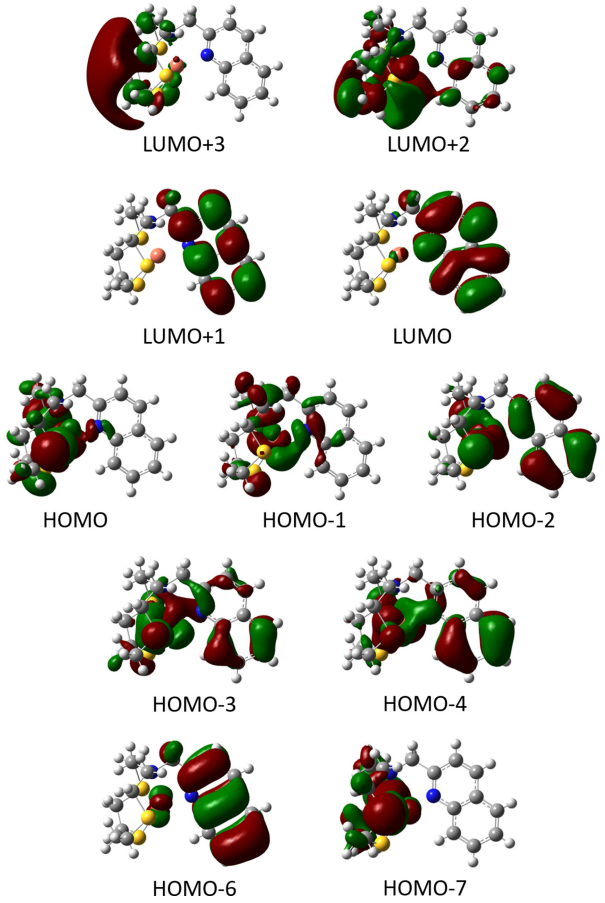

Figure 8. Frontier molecular orbitals for the model system **7a**.

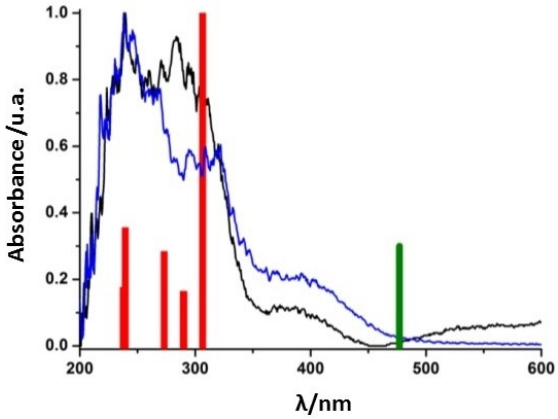

Figure 9. Experimental Uv-vis solid state absorption spectrum for **7** (blue line), and **9** (black line), and TD-DFT singlet-singlet calculated excitations (red bars) for model system **7a**. The lowest singlet-triplet (green bar) excitation for model 7a is also included (the green bar only repesents the energy of the computed singlet-triplet transition, since the oscillator strength cannot be estimated).

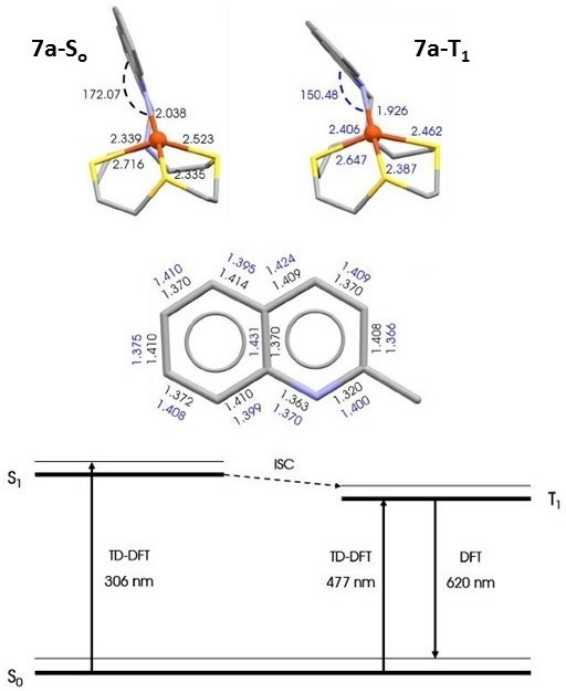

Figure 10. Main structural parameters for the model system **7a** in the fundamental state S_o (upper-left) and in the triplet state T_1 (upper-right), comparison of the structural parameters for the quinoline moiety in **7a**-S_0 (black) and **7a**-T_1 (blue) (middle), energy diagram of the computed results for the model **7a** (down).

Since the lifetimes for complexes **7** and **9** lie in the range of microseconds, the first singlet-triplet excitation was also computed for **7a**. It appears at 477.09 nm and has two main contributions, in which the electron arises from HOMO-4 and HOMO-2 and arrives to LUMO, therefore corresponding to a charge-transfer from the macrocyclic + Cu(I) moiety to the quinoline fragment (Tables S7, S8).

The singlet-triplet calculated excitation is red-shifted with respect to the band at lower energy observed in the Uv-vis spectra of **7** and **9** recorded in the solid state (Figure 9). This feature is not unusual for transitions originating from a charge-transfer that DFT and TD-DFT tend to underestimate.

In order to get a deeper insight into the origin of the phosphoresce emission observed for **7** and **9**, the structure of the first excited triplet state of **7a** was optimized and the results are shown in Figure 10. The most significant distortion observed in the optimized structure of **7a-T$_1$** with respect to the structure of **7a-S$_0$** is represented by the different position of the quinoline moiety with respect to the rest of the $[Cu(\mathbf{L4})]^+$ cation, which can be evaluated by the change in the calculated angle centroid–N_Q–Cu (150.48° in **7a-T$_1$**, 172.02° in **7a-S$_0$**).

Considering the coordination bond distances, both Cu–N/S and Cu–N_Q undergo significant changes on passing from the fundamental state S_0 to the first triplet state T_1. In particular, the latter suffers the highest distortion by changing from 2.038 (**7a-S$_0$**) to 1.926 Å (**7a -T$_1$**), with the C–N_Q distance that increases from 1.320 (**7a-S$_0$**) to 1.400 Å (**7a-T$_1$**). These distortions agree with the hypothesis that the phosphorescent properties of **7** and **9** might be related to a transition involving the quinoline pendant moiety together with a charge-transfer involving mainly the quinoline moiety and the copper(I) centre in the $[Cu(\mathbf{L4})]^+$ cation. We have computed the singly-occupied molecular orbitals SOMO and SOMO-1, which correspond to the orbitals involved in the electronic relaxation responsible for the phosphorescence of complex **7** (see Figure S16 in SI). Both MOs consist of π orbitals located on the pendant quinoline moiety of the **L4** ligand, with a small contribution of Cu to SOMO-1. This would be in agreement with a forbidden intraligand transition ^{3}IL admixed with a ligand-to-metal charge transfer transition ^{3}LMCT from the quinoline fragment to the Cu(I) centre.

Finally, the theoretical emission for the model **7a** was evaluated by calculating at DFT level the energy of the triplet state T_1 and the energy of the fundamental state S_0 at the optimized structure of the excited state (Figure 10).

The difference between the two indicates a theoretical emission at 620 nm, which is slightly red-shifted with respect the experimental values of 595 and 596 nm recorded for **7** and **9**, respectively.

Conclusions

In this paper we have described the structural and optical properties of the heteronuclear Au(I)/Cu(I) compounds obtained by reacting $[\{Au(C_6X_5)_2\}_2Cu_2(MeCN)_2]_n$ (X = F, Cl) with the thioethers crowns **L1**–**L3** (featuring different ring sizes and number of S-donors) and the quinoline functionalized pendant arm derivatives of the mixed thia-aza 12-membered macrocycles [12]aneNS$_3$ and [12]aneN$_2$S$_2$, **L4** and **L5**, respectively. In contrast with the compounds previously obtained considering Ag(I) and Tl(I) as closed-shell metal ions (many of them polynuclear or polymeric), following identical synthetic strategy and experimental conditions, only with **L1** and **L2** was it possible to prepare dinuclear complexes featuring a

Au(I)···Cu(I) interaction (see Scheme 2). In most cases ionic compounds were isolated featuring $[Cu(\mathbf{L})]^+$ complex cations balanced by the anions $[Au(C_6X_5)_2]^-$ with no metallophilic interactions between them, but they all displaying non-classical C–H···Au hydrogen interactions. The absence of metallophilic interactions could be determined by the different dimensions and stereochemical demands of the three d^{10} metal ions, independently of nature of the halogen atom in the aurate(I) anion and the ring sizes and donor sets in the macrocyclic ligands. As expected, the luminescence properties of the structurally characterized compounds featuring Au(I)···Cu(I) metallophilic interactions, namely [{Au(C_6F_5)$_2$}{Cu(**L1**)}] (**1**), [{Au(C_6Cl_5)$_2$}{Cu(**L1**)}] (**4**), and [Cu(**L2**)][Au(C_6Cl_5)$_2$] (**5**), are directly correlated to transition processes involving the two interacting metal units (following confirmation by theoretical calculations). In the case of the complexes [Cu(**L4**)][Au(C_6F_5)$_2$] (**7**) and [Cu(**L4**)][Au(C_6Cl_5)$_2$] (**9**), the other two luminescent compounds isolated, their phosphorescent emission appears to be related to a $T_1 \rightarrow S_0$ charge-transfer involving mainly the copper(I) centre and the quinoline moiety in the $[Cu(\mathbf{L4})]^+$ cation, with the structure of the excited triplet state being highly distorted as compared to the fundamental S_0 state, and the aurate(I) counter anion being not involved in the emissive process.

Experimental Section

$[\{Au_2Cu_2(C_6X_5)_2\}(CH_3CN)_2]_n$ (X = F,[56] Cl[57]), the ligands **L1**–**L3**,[71–73] and **L4** and **L5**[54] were prepared according to the literature. C, H, N, and S analyses were carried out with a Perkin-Elmer 240 C microanalyzer. ^{1}H- and ^{19}F-NMR spectra were recorded on a Bruker Avance 400 in THF–D8 or acetone-D6 solutions. Chemical shifts are quoted relative to $SiMe_4$ (^{1}H) and $CFCl_3$ (^{19}F) external references. Mass spectra were recorded on a Bruker Microflex MALDI-TOF using dithranol (DIT) or11-dicyano-4-tert-butylphenyl-3-methylbutadiene (DCTB) as the matrix. Infrared spectra were recorded on either a Nicolet Nexus FT-IR using Nujol mulls between polyethylene sheets, or on Perkin Elmer FT-IR spectrometer equipped with an ATR accessory, in the ranges 4000–200 or 4000–500 cm^{-1}, respectively. Molar conductivities were measured in *ca.* 5×10^{-4} M acetone solutions by using a Jenway 4510 digital conductivity meter.

Absorption spectra in solution were recorded on a Hewlett-Packard 8453 diode array UV-vis spectrophotometer. Diffuse reflectance UV-vis spectra of pressed powder samples diluted with KBr were recorded on a Shimadzu (UV3600 spectrophotometer with a Harrick Praying Mantis accessory) and recalculated following the Kubelka-Munk function.

Excitation and emission spectra in the solid state were recorded with a Jobin-Yvon Horiba Fluorolog 3–22 Tau-3 spectrofluorimeter. Lifetime measurements were recorded with a Datastation HUB–B with a nanoLED controller and DAS6 software. The nanoLED employed for lifetime measurements was one of 370 nm with pulse lengths of 0.8–1.4 ns. The lifetime data were fitted with the Jobin-Yvon software package. Measurements at 77 K were registered with an Oxford Cryostat Optistat DN with an accessory for solid samples.

[{Au(C_6F_5)$_2$}{Cu(L1)}] (1), [Cu(L2)][Au(C_6F_5)$_2$] (2) and [Cu(L3)][Au(C_6F_5)$_2$]$_2$ (3): $[\{Au_2Cu_2(C_6F_5)_4\}(CH_3CN)_2]_n$ (50 mg, 0.039 mmol) was added to a solution of $\mathbf{L}_1$ (14.2 mg, 0.079 mmol) or **L2** (21.1 mg, 0.079 mmol) or **L3** (18.9 mg, 0.039 mmol) in THF (20 mL). The resulting colourless solutions were stirred at room temperature for 2 h. The volume of the solutions was reduced to approximately 2 mL under reduced pressure to afford upon addition of *n*-hexane white precipitates that were isolated by filtration with 69 (**L1**), 74 (**L2**), and 79% (**L3**) yields, respectively.

Compound 1: Anal. Found (Calcd.) for $C_{18}H_{12}AuCuF_{10}S_3$ (774.98 g/mol): C 27.46 (27.90); H 2.10 (1.56); S 13.17 (12.41). ^{1}H-NMR (THF-[D_8], 400 MHz): δ_H 2.93 ppm (s, 12H). ^{19}F-NMR (THF-[D_8], 376 MHz): δ_F −115.6 (m, 2F, F_o), −163.4 (t, $^3J_{F\text{-}F}$ = 20 Hz, 1F, F_p), −166.7 ppm (m, 2F, F_m). MALDI-TOF(−) m/z = 531 $[Au(C_6F_5)_2]^-$; MALDI-TOF(+) m/z = 243 $[Cu(\mathbf{L1})]^+$. FT-IR (ATR): ν($[Au(C_6F_5)_2]^-$) at 1502, 950 and 782 cm^{-1}; other selected peaks at 1685, 1444, 1333, 1037, 593 cm^{-1}. Λ_M (acetone): 105 $\Omega^{-1}\,cm^2\,mol^{-1}$.

Compound 2: Anal. Found (Calcd.) for $C_{22}H_{20}AuCuF_{10}S_4$ (863.15 g/mol): C 30.75 (30.61); H 2.65 (2.34); S 14.95 (14.86). ^{1}H-NMR (THF-[D_8], 400 MHz): δ_H 2.01 (quintet, $^3J_{H\text{-}H}$ = 2 Hz, 4H), 2.73 (t, $^3J_{H\text{-}H}$ = 2 Hz, 8H), 2.85 ppm (s, 8H). ^{19}F-NMR (THF-[D_8], 376 MHz): δ_F −115.0 (m, 2F, F_o), −164.8 (t, $^3J_{F\text{-}F}$ = 20 Hz, 1F, F_p), −165.6 ppm (m, 2F, F_m). MALDI-TOF(−) m/z = 531 $[Au(C_6F_5)_2]^-$; MALDI-TOF(+) m/z = 331 $[Cu(\mathbf{L2})]^+$. FT-IR (ATR): ν($[Au(C_6F_5)_2]^-$) at 1501, 950 and 781 cm^{-1}; other selected peaks at 1685, 1445, 1334, 1037 cm^{-1}. Λ_M (acetone): 138 $\Omega^{-1}\,cm^2\,mol^{-1}$.

Compound 3: Anal. Found (Calcd.) for $C_{40}H_{32}Au_2Cu_2F_{20}S_8$ (1670.20 g/mol): C 29.20 (28.76); H 2.05 (1.93); S 15.58 (15.36). ^{1}H-NMR (THF-[D_8], 400 MHz): δ_H 3.07 ppm (s, 32H). ^{19}F-NMR (THF-[D_8], 376 MHz): δ_F −115.1 (m, 4F, F_o), −163.9 (t, $^3J_{F\text{-}F}$ = 20 Hz, 1F, F_p), −165.1 ppm (m, 2F, F_m). MALDI-TOF(−) m/z = 531 $[Au(C_6F_5)_2]^-$; MALDI-TOF(+) m/z = 543 $[Cu(\mathbf{L3})]^+$. FT-IR (ATR): ν($[Au(C_6F_5)_2]^-$) at 1497, 951 and 779 cm^{-1}; other selected peaks at 1687, 1444, 1407, 1259, 1055, 815 cm^{-1}. Λ_M (acetone): 172 $\Omega^{-1}\,cm^2\,mol^{-1}$.

[{Au(C_6Cl_5)$_2$}{Cu(L1)}] (4), [Cu(L2)][Au(C_6Cl_5)$_2$] (5) and [Cu(L3)][Au(C_6Cl_5)$_2$]$_2$ (6): $[\{Au_2Cu_2(C_6Cl_5)_4\}(CH_3CN)_2]_n$ (50 mg, 0.031 mmol) was added to a solution of **L1** (11.3 mg, 0.062 mmol) or **L2** (16.8 mg, 0.062 mmol) or **L3** (15.0 mg, 0.031 mmol) in THF (20 mL). The resulting yellow solutions were stirred at room temperature for 2 h, turning colourless after this period of time. The volume of the solutions was reduced to approximately 2 mL under reduced pressure to afford upon addition of *n*-hexane white precipitates (or light yellow in the case of $\mathbf{L}_2$) that were isolated by filtration with 82 (**L1**), 85 (**L2**), and 92% (**L3**) yields, respectively.

Compound 4: Anal. Found (Calcd.) for $C_{18}H_{12}AuCl_{10}CuS_3$ (939.52 g/mol): C 23.40 (23.01); H 1.86 (1.29); S 11.00 (10.24). ^{1}H-NMR (THF-[D_8], 400 MHz): δ_H 2.88 ppm (s, 12H). MALDI-TOF(−) m/z = 695 $[Au(C_6Cl_5)_2]^-$; MALDI-TOF(+) m/z = 243 $[Cu(\mathbf{L1})]^+$. FT-IR (ATR): ν($[Au(C_6Cl_5)_2]^-$) at 834 and 611 cm^{-1}; other selected peaks at 1425, 1389, 1306, 1278, 1204,1056, 667 cm^{-1}. Λ_M (acetone): 126 $\Omega^{-1}\,cm^2\,mol^{-1}$.

Compound 5: Anal. Found (Calcd.) for $C_{22}H_{20}AuCl_{10}CuS_4$ (1027.70 g/mol): C 25.34 (25.71); H 2.21 (1.96); S 12.43 (12.81). ^{1}H-NMR (THF-[D_8], 400 MHz): δ_H 1.93 (quintet, $^3J_{H\text{-}H}$ = 2 Hz, 4H), 2.64 (t, $^3J_{H\text{-}H}$ = 2 Hz, 8H), 2.76 ppm (s, 8H). MALDI-TOF(−) m/z = 695 $[Au(C_6Cl_5)_2]^-$; MALDI-TOF(+) m/z = 331 $[Cu(\mathbf{L2})]^+$. FT-IR (ATR): ν($[Au(C_6Cl_5)_2]^-$) at 835 and 613 cm^{-1}; other selected peaks at 1425, 1314, 1278, 1222, 1065, 685 cm^{-1}. Λ_M (acetone): 112 $\Omega^{-1}\,cm^2\,mol^{-1}$.

Compound 6: Anal. Found (Calcd.) for $C_{40}H_{32}Au_2Cl_{20}Cu_2S_8$ (1999.29 g/mol): C 24.49 (24.03); H 1.86 (1.61); S 12.68 (12.83). ^{1}H-NMR (THF-[D_8], 400 MHz): δ_H 2.82 ppm (s, 32H). MALDI-TOF(−) m/z = 695 $[Au(C_6F_5)_2]^-$; MALDI-TOF(+) m/z = 543 $[Cu(\mathbf{L3})]^+$. FT-IR (ATR): ν($[Au(C_6Cl_5)_2]^-$) at 832 and 617 cm^{-1}; other selected peaks at 1463, 1306, 1278, 1083, 870, 741, 667 cm^{-1}. Λ_M (acetone): 199 $\Omega^{-1}\,cm^2\,mol^{-1}$.

[Cu(L4)][Au(C_6F_5)$_2$] (7) and [Cu(L5)][Au(C_6F_5)$_2$] (8): [{$Au_2Cu_2(C_6F_5)_4$}(CH_3CN)$_2$]$_n$ (50 mg, 0.039 mmol) was added to a solution of **L4** (28.7 mg, 0.079 mmol) or **L5** (38.4 mg, 0.079 mmol) in THF (20 mL). The resulting brown solutions were stirred at room temperature for 2 h. The volume of the solutions was reduced to approximately 2 mL under reduced pressure to afford upon addition of Et_2O (**L4**) *n*-hexane (**L5**) brown precipitates that were isolated by filtration with 80 (**L4**) and 61% (**L5**) yields, respectively.

Compound 7: Anal. Found (Calcd.) for $C_{30}H_{24}AuCuF_{10}N_2S_3$ (959.22 g/mol): C 37.33 (37.56); H 2.88 (2.52); N 3.21 (2.92); S 10.03 (10.03). ^{1}H-NMR (acetone-[D_6], 400 MHz): δ_H 3.01-3.23 (m, 16H), 4.17 (s, 2H), 7.64 (d, 1H), 7.73 (t, 1H), 7.92 (t, 1H), 8.10 (d, 1H), 8.46 (d, 1H), 8.57 ppm (d, 1H). ^{19}F-NMR (acetone-[D_6], 376 MHz): δ_F −115.7 (m, 2F, F_o), −164.6 (t, $^3J_{F\text{-}F}$ = 20 Hz, 1F, F_p), −165.5 ppm (m, 2F, F_m). MALDI-TOF(−) m/z = 531 [Au(C_6F_5)$_2$]$^-$; MALDI-TOF(+) m/z = 427 [Cu(**L4**)]$^+$. FT-IR (ATR): ν([Au(C_6F_5)$_2$]$^-$) at 1497, 952 and 780 cm^{-1}, ν(**L4**) at 1590–1640 (br, w) cm^{-1}; other selected peaks at 1407, 1046, 806 cm^{-1}. Λ_M (acetone): 106 Ω^{-1} cm^2 mol^{-1}.

Compound 8: Anal. Found (Calcd.) for $C_{40}H_{32}AuCuF_{10}N_4S_2$ (1083.34 g/mol): C 44.62 (44.35); H 3.38 (2.98); N 5.27 (5.17); S 5.44 (5.92). ^{1}H-NMR (acetone-[D_6], 400 MHz): δ_H 2.95-3.29 (m, 16H), 4.27 (s, 4H), 7.62 (t, 2H), 7.73 (t, 2H), 7.86(d, 2H), 8.02 (d, 2H), 8.20 (d, 2H), 8.50 ppm (d, 2H). ^{19}F-NMR (acetone-[D_6], 376 MHz): δ_F −115.7 (m, 2F, F_o), −164.6 (t, $^3J_{F\text{-}F}$ = 20 Hz, 1F, F_p), −165.5 ppm (m, 2F, F_m). MALDI-TOF(−) m/z = 531 [Au(C_6F_5)$_2$]$^-$; MALDI-TOF(+) m/z = 551 [Cu(**L5**)]$^+$. FT-IR (ATR): ν([Au(C_6F_5)$_2$]$^-$) at 1497, 948 and 778 cm^{-1}, ν(**L5**) at 1570–1740 (br, w) cm^{-1}; other selected peaks at 1445, 1120, 1046, 815 cm^{-1}. Λ_M (acetone): 130 Ω^{-1} cm^2 mol^{-1}.

[Cu(L4)][Au(C_6Cl_5)$_2$] (9) and [Cu(L5)][Au(C_6Cl_5)$_2$] (10): [{$Au_2Cu_2(C_6Cl_5)_4$}(CH_3CN)$_2$]$_n$ (50 mg, 0.031 mmol) was added to a solution of **L4** (22.8 mg, 0.062 mmol) or **L5** (30.68 mg, 0.062 mmol) in THF (20 mL). The resulting brown solutions were stirred at room temperature for 2 h turning yellow in the case of **L4** and brown in the case of **L5**. The volume of the solutions was reduced to approximately 2 mL under reduced pressure to afford upon addition of *n*-hexane a yellow precipitate in the case of the reaction with **L4** and a brown precipitate in the case of the reaction with **L5**, which were isolated by filtration with 82 (**L4**) and 56% (**L5**) yields, respectively.

Compound 9: Anal. Found (Calcd.) for $C_{30}H_{24}AuCl_{10}CuN_2S_3$ (1123.76 g/mol): C 31.96 (32.06); H 2.44 (2.15); N 2.47 (2.49); S 8.26 (8.56). ^{1}H-NMR (acetone-[D_6], 400 MHz): δ_H 3.01-3.20 (m, 16H), 4.16 (s, 2H), 7.64 (d, 1H), 7.73 (t, 1H), 7.92 (t, 1H), 8.09 (d, 1H), 8.46 (d, 1H), 8.57 ppm (d, 1H). MALDI-TOF(−) m/z = 695 [Au(C_6Cl_5)$_2$]$^-$; MALDI-TOF(+) m/z = 427 [Cu(**L4**)]$^+$. FT-IR (ATR): ν([Au(C_6Cl_5)$_2$]$^-$) at 833 and 612 cm^{-1}, ν(**L4**) at 1560–1620 (br, w) cm^{-1}; other selected peaks at 1418, 1309, 1282, 1091, 909, 664 cm^{-1}. Λ_M (acetone): 108 Ω^{-1} cm^2 mol^{-1}.

Compound 10: Anal. Found (Calcd.) for $C_{40}H_{32}AuCl_{10}CuN_4S_2$ (1083.34 g/mol): C 38.60 (30.50); H 2.64 (2.58); N 4.33 (4.49); S 5.19 (5.14). ^{1}H-NMR (acetone-[D_6], 400 MHz): δ_H 2.96-3.29 (m, 16H), 4.27 (s, 4H), 7.63 (t, 2H), 7.74 (t, 2H), 7.86(d, 2H), 8.03 (d, 2H), 8.20 (d, 2H), 8.49 ppm (d, 2H). MALDI-TOF(−) m/z = 695 [Au(C_6Cl_5)$_2$]$^-$; MALDI-TOF(+) m/z = 551 [Cu(**L5**)]$^+$. FT-IR (ATR): ν([Au(C_6Cl_5)$_2$]$^-$) at 829 and 614 cm^{-1}, ν(**L5**) at 1560–1725 (br, w) cm^{-1}; other selected peaks at 1445, 1309, 1281, 1091, 773, 745, 673 cm^{-1}. Λ_M (acetone): 126 Ω^{-1} cm^2 mol^{-1}.

Crystallography

Details of data collection and refinement are provided in Table S1 in the SI, only special features are noted here. Crystals were mounted in inert oil on glass fibers and transferred to the cold gas stream of a Nonius Kappa CCD diffractometer equipped with an Oxford Instruments low-temperature attachment. Data were collected using monochromated MoK_α radiation (λ = 0.71073 Å). Scan type: ω and ϕ. Absorption effects were treated by semiempirical corrections based on multiple scans. The structures were solved and refined on F^2 using the SHELX program.[74] All the non-hydrogen atoms were refined anisotropically. The hydrogen atoms were included using a riding model.

Deposition Numbers 2286294 (for **1**), 2286295 (for **2**), 2286296 (for **3**), 2286297 (for **4**), 2286298 (for **5**), 2286299 (for **7**), 2286300 (for **8**·0.5***n*-hexane**), 2286301 (for **9**), 2286302 (for **10**) contain the supplementary crystallographic data for this paper. These data are provided free of charge by the joint Cambridge Crystallographic Data Centre and Fachinformationszentrum Karlsruhe Access Structures service.

Computational details

All calculations were carried out using Gaussian 09 program package.[75] DFT and Time Dependent TD-DFT calculations were carried out with using the PBE functional.[76] The following basis set combinations were employed for the metals Au and Cu: the 19-VE pseudopotentials from Stuttgart and the corresponding basis sets augmented with two f polarization functions,[77] respectively. The rest of the atoms were treated with SVP basis sets.[78,79] All the calculations for **1a**, **4a**, and **5a** were performed on model systems built from their corresponding X-ray structures. For **7a** calculations were performed on the optimized structure at DFT level of the model system. Topological calculations (NCI) were computed with Multiwfn[80] and visualized with VMD.[81]

Acknowledgements

VL thanks the Università degli Studi di Cagliari for financial support. JML-d-L, MEO and MM acknowledge the DGI MICINN/FEDER (project number PID2022-139739NB-I00 (AEI/FEDER, UE)) and by "ERDF A way of making Europe".

Conflict of Interests

The authors declare no conflict of interest.

Data Availability Statement

The data that support the findings of this study are available in the supplementary material of this article.

Keywords: thioether crown · quinoline · gold · copper · metallophilic interactions

[1] (Ed.: A. Laguna) *Modern Supramolecular Gold Chemistry: Gold-Metal Interactions and Applications*, Wiley-VCH, Weinheim, Germany, **2008**, ISBN 978-352732095.
[2] (Ed.: F. Mohr) *Gold Chemistry: Applications and Future Directions in the Life Sciences*, Wiley-VCH, Weinheim, Germany, **2009**, ISBN 978-3527320868.

[3] C.-K. Chan, C.-X. Guo, K.-K. Cheung, D. Li, C.-M. Che, *J. Chem. Soc. Dalton Trans.* **1994**, 3677–3682.
[4] V. J. Catalano, J. M. López-de-Luzuriaga, M. Monge, M. E. Olmos, D. Pascual, *Dalton Trans.* **2014** *43*, 16486–16497.
[5] E. J. Fernández, A. Laguna, J. M. López-de-Luzuriaga, M. Monge, M. Montiel, M. E. Olmos, M. Rodríguez-Castillo, *Dalton Trans.* **2009**, 7509–7518.
[6] E. J. Fernández, M. C. Gimeno, A. Laguna, J. M. López-de-Luzuriaga, M. Monge, P. Pyykkö, D. Sundholm, *J. Am. Chem. Soc.* **2000**, *122*, 7287–7293.
[7] M. Gil-Moles, M. C. Gimeno, J. M. López-de-Luzuriaga, M. Monge, M. E. Olmos, *Dalton Trans.* **2019**, *48*, 5149–5155.
[8] E. J. Fernández, J. M. López-de-Luzuriaga, M. Monge, M. A. Rodríguez, O. Crespo, M. C. Gimeno, A. Laguna, P. G. Jones, *Chem. Eur. J.* **2000**, *6*, 636–644.
[9] D. Rios, M. M. Olmstead, A. L. Balch, *Inorg. Chem.* **2009**, *48*, 5279–5287.
[10] J. Fernandez-Cestau, R. J. Rama, L. Rocchigiani, B. Bertrand, E. Lalinde, M. Linnolahti, M. Bochmann, *Inorg. Chem.* **2019**, *58*, 2020–2020.
[11] A. Burini, R. Bravi, J. P. Fackler Jr., R. Galassi, T. A. Grant, M. A. Omary, B. R. Pietroni, R. Staples, *Inorg. Chem.* **2000**, *39*, 3158–3165.
[12] S. Wang, G. Garzón, C. King, J. C. Wang, J. P. Fackler Jr., *Inorg. Chem.* **1989**, *28*, 4623–4629.
[13] T. P. Seifert, N. D. Knoefel, T. J. Feuerstein, K. Reiter, S. Lebedkin, M. T. Gamer, A. C. Boukis, F. Weigend, M. M. Kappes, P. W. Roesky, *Chem. Eur. J.* **2019**, *25*, 3799–3808.
[14] O. Crespo, E. J. Fernández, A. Laguna, J. M. López-de-Luzuriaga, A. Mendía, M. Monge, M. E. Olmos, P. G. Jones, *Chem. Commun.* **1998**, 2233–2234.
[15] V. J. Catalano, B. L. Bennett, H. M. Kar, B. C. Noll, *J. Am. Chem. Soc.* **1999**, *121*, 10235–10236.
[16] S. Wang, J. P. Fackler Jr., C. King, J. C. Wang, *J. Am. Chem. Soc.* **1988**, *110*, 3308–3310.
[17] M. Arca, R. Donamaría, M. C. Gimeno, V. Lippolis, J. M. López-de-Luzuriaga, E. Manso, M. Monge, M. E. Olmos, *Dalton Trans.* **2015**, *44*, 6719–6730.
[18] L. H. Gade, *Angew. Chem. Int. Ed. Engl.* **2001**, *40*, 3573–3575.
[19] R. Echeverría, J. M. López-de-Luzuriaga, M. Monge, M. E. Olmos, *Chem. Sci.* **2015**, *6*, 2022–2026.
[20] J. M. López-de-Luzuriaga, M. Monge, S. Moreno, M. E. Olmos, M. Rodríguez-Castillo, *Angew. Chem. Int. Ed. Engl.* **2020**, *60*, 640–644.
[21] R. Echeverría, J. M. López-de-Luzuriaga, M. Monge, S. Moreno, M. E. Olmos, M. Rodríguez-Castillo, *Chem. Commun.* **2018**, *54*, 295–298.
[22] A. Burini, J. P. Fackler Jr., R. Galassi, T. A. Grant, M. A. Omary, M. A. Rawashdeh-Omary, B. R. Pietroni, R. J. Staples, *J. Am. Chem. Soc.* **2000**, *122*, 11264–1126.
[23] J. M. López-de-Luzuriaga, M. Monge, M. E. Olmos, D. Pascual, *Inorg. Chem.* **2014**, *53*, 1275–1277.
[24] J. M. López-de-Luzuriaga, M. Monge, M. E. Olmos, D. Pascual, T. Lasanta, *Chem. Commun.* **2011**, *47*, 6795–6797.
[25] E. J. Fernández, A. Laguna, J. M. López-de-Luzuriaga, M. Monge, M. Nema, M. E. Olmos, J. Pérez, C. Silvestru, *Chem. Commun.* **2007**, 571–573.
[26] R. V. Bojan, J. M. López-de-Luzuriaga, M. Monge, M. E. Olmos, R. Echeverría, O. Lehtonen, D. Sundholm, *ChemPlusChem* **2014**, *79*, 67–76.
[27] J. M. López-de-Luzuriaga, M. Monge, M. E. OLmos, D. Pascual, *Organom.* **2015**, *34*, 3029–3038.
[28] H. Schmidbaur, H. G. Raubenheimer, *Angew. Chem. Int. Ed. Engl.* **2020**, *59*, 14748–14771.
[29] H. Schmidbaur, A. A. Schier, *Chem. Soc. Rev.* **2008**, *37*, 1931–1951.
[30] H. Schmidbaur, A. A. Schier, *Chem. Soc. Rev.* **2012**, *41*, 370–412.
[31] P. Pyykkö, *Chem. Rev.* **1997**, *97*, 597–636.
[32] P. Pyykkö, *Chem. Soc. Rev.* **2008**, *37*, 1967–1997.
[33] A. J. Blake, R. Donamaría, V. Lippolis, J. M. Lopez-de-Luzuriaga, M. Monge, M. E. Olmos, A. Seal, J. A. Weinstein, *Inorg. Chem.* **2019**, *58*, 4954–4961.
[34] R. Donamaría, V. Lippolis, J. M. López-de-Luzuriaga, M. Monge, M. E. Olmos, *Comp. Theor. Chem.* **2014**, *1030*, 53–58.
[35] J. M. Forward, J. P. Fackler Jr., Z. Assefa, in *Photophysical and Photochemical Properties of Gold(I) Complexes*, (Eds.: D. M. Roundhill, J. P., Jr. Fackler) in Optoelectronic Properties of Inorganic Compounds, Springer, US, **1999**, ISBN 978-1475761016.
[36] V. W.-W. Yam, V. K.-M. Au, S. Y.-L. Leung, *Chem. Rev.* **2015**, *115*, 7589–7728.
[37] M. J. Katz, K. Sakai, D. B. Leznoff, *Chem. Soc. Rev.* **2008**, *37*, 1884–1895.
[38] X. Zhang, B. Li, Z.-H. Chen, Z.-N. Chen, *J. Mater. Chem.* **2012**, *22*, 11427–11441.
[39] C. E. Strasser, V. J. Catalano, *J. Am. Chem. Soc.* **2010**, *132*, 10009–10011.
[40] M. Ganguly, J. Jana, A. Pal, T. Pal, *RSC Adv.* **2016**, *6*, 17683–17703.
[41] E. J. Fernández, A. Laguna, J. M. López-de-Luzuriaga, *Dalton Trans.* **2007**, 1969–1981.
[42] J. M. López-de-Luzuriaga, M. Monge, M. E. Olmos, *Dalton Trans.* **2017**, *46*, 2046–2067.
[43] R. J. Roberts, D. Le, D. B. Leznoff, *Chem. Commun.* **2015**, *51*, 14299–14302.
[44] S. H. Lim, M. M. Olmstead, A. L. Balch, *J. Am. Chem. Soc.* **2011**, *133*, 10229–10238.
[45] E. J. Fernández, J. M. López-de-Luzuriaga, M. Monge, M. E. Olmos, J. Pérez, A. Laguna, A. A. Mohammed Jr., J. P. Fackler, *J. Am. Chem. Soc.* **2003**, *125*, 2022–2023.
[46] E. J. Fernández, J. M. López-de-Luzuriaga, M. Monge, M. E. Olmos, R. C. Puelles, A. Laguna, A. A. Mohammed Jr., J. P. Fackler, *Inorg. Chem.* **2008**, *47*, 8069–8076.
[47] A. J. Blake, R. Donamaría, V. Lippolis, J. M. Lopez-de-Luzuriaga, E. Manso, M. Monge, M. E. Olmos, *Inorg. Chem.* **2014**, *53*, 10471–10484.
[48] A. J. Blake, R. Donamaría, E. J. Fernández, T. Lasanta, V. Lippolis, J. M. Lopez-de-Luzuriaga, E. Manso, M. Monge, M. E. Olmos, *Dalton Trans.* **2013**, *42*, 11559–11570.
[49] R. Donamaría, M. C. Gimeno, V. Lippolis, J. M. Lopez-de-Luzuriaga, M. Monge, M. E. Olmos, *Inorg. Chem.* **2016**, *55*, 11299–11310.
[50] R. Donamaría, V. Lippolis, J. M. Lopez-de-Luzuriaga, M. Monge, M. Nieddu, M. E. Olmos, *Inorg. Chem.* **2017**, *56*, 12551–12563.
[51] R. Donamaría, V. Lippolis, J. M. Lopez-de-Luzuriaga, M. Monge, M. Nieddu, M. E. Olmos, *Chem. Eur. J.* **2018**, *24*, 13740–13743.
[52] R. Donamaría, V. Lippolis, J. M. Lopez-de-Luzuriaga, M. Monge, M. Nieddu, M. E. Olmos, *Eur. J. Inorg. Chem.* **2021**, 4552–4559.
[53] R. Donamaría, V. Lippolis, J. M. Lopez-de-Luzuriaga, M. Monge, M. Nieddu, M. E. Olmos, *Inorg. Chem.* **2020**, *59*, 6398–6409.
[54] R. Donamaría, V. Lippolis, J. M. Lopez-de-Luzuriaga, M. Monge, M. Nieddu, M. E. Olmos, *Inorg. Chem.* **2018**, *57*, 11099–11112.
[55] R. Donamaría, V. Lippolis, J. M. Lopez-de-Luzuriaga, M. Monge, M. Nieddu, M. E. Olmos, *Dalton Trans.* **2020**, *49*, 10983–10993.
[56] E. J. Fernández, A. Laguna, J. M. López-de-Luzuriaga, M. Monge, M. Montiel, M. E. Olmos, M. Rodríguez-Castillo, *Organom.* **2006**, *25*, 3639–3646.
[57] R. Donamaría, E. J. Fernández, J. M. López-de-Luzuriaga, M. Monge, M. E. Olmos, D. Pascual, M. Rodríguez-Castillo, *Dalton Trans.* **2017**, *46*, 10941–10949.
[58] E. J. Fernández, A. Laguna, J. M. López-de-Luzuriaga, M. Monge, M. Montiel, M. E. Olmos, *Inorg. Chem.* **2005**, *44*, 1163–1165.
[59] M. Rodríuez-Castillo, M. Monge, J. M. López-de-Luzuriaga, M. E. Olmos, A. Laguna, F. Mendizabal, *Comp. Theor. Chem.* **2011**, *965*, 163–167.
[60] J. M. López-de-Luzuriaga, M. Monge, M. E. Olmos, M. Rodríuez-Castillo, A. Laguna, F. Mendizabal, *Theor. Chem. Acc.* **2011**, *129*, 593–602.
[61] A. W. Addison, T. Nageswara Rao, J. Reedijk, J. van Rijn, G. C. Verschoor, *J. Chem. Soc. Dalton Trans.* **1984**, 1349–1356.
[62] H.-J. Küppers, K. Wieghardt, Y.-H. Tsay, C. Krüger, B. Nuber, J. Weiss, *Angew. Chem. Int. Ed. Engl.* **1987**, *26*, 575–576.
[63] J. A. Clarkson, R. Yagbasan, P. J. Blower, S. R. Cooper, *J. Chem. Soc. Chem. Commun.* **1989**, 1244–1245.
[64] A. J. Blake, R. O. Gould, A. J. Holder, A. J. Lavery, M. Schröder, *Polyhedron* **1990**, *9*, 2919–2924.
[65] M. D. Glick, D. P. Gavel, L. L. Diaddario, D. B. Rorabacher, *Inorg. Chem.* **1976**, *15*, 1190–1193.
[66] E. R. Dockal, L. L. Diaddario, M. D. Glick, D. B. Rorabacher, *J. Am. Chem. Soc.* **1977**, *99*, 4530–4532.
[67] S.-Z. Hu, Z.-H. Zhou, Z.-X. Xie, B. E. Robertson, *Z. Kristallogr.* **2014**, *229*, 517–523.
[68] S. Álvarez, *Dalton Trans.* **2013**, *42*, 8617–8636.
[69] https://webelements.com.
[70] A. J. Blake, A. taylor, M. Schröder, *Polyhedron* **1990**, *9*, 2911–2918.
[71] D. Sellmann, L. Zapf, *Angew. Chem.* **1984**, *96*, 799–800.
[72] J. Buter, R. M. Kellog, *J. Org. Chem.* **1981**, *46*, 4481–4485.
[73] J. J. H. Edema, J. Buter, R. M. Kellog, *Tetrahedron* **1991**, *50*, 2095–2098.
[74] G. M. Sheldrick, *Acta Crystallogr. Sect. C* **2015**, *71*, 3–8.
[75] M. J. Frisch, G. W. Trucks, H. B. Schlegel, G. E. Scuseria, M. A. Robb, J. R. Cheeseman, G. Scalmani, V. Barone, B. Mennucci, G. A. Petersson, H. Nakatsuji, M. Caricato, X. Li, H. P. Hratchian, A. F. Izmaylov, J. Bloino, G. Zheng, J. L. Sonnenberg, M. Hada, M. Ehara, K. Toyota, R. Fukuda, J. Hasegawa, M. Ishida, T. Nakajima, Y. Honda, O. Kitao, H. Nakai, T. Vreven,

J. A. Montgomery Jr., J. E. Peralta, F. Ogliaro, M. Bearpark, J. J. Heyd, E. Brothers, K. N. Kudin, V. N. Staroverov, R. Kobayashi, J. Normand, K. Raghavachari, A. Rendell, J. C. Burant, S. S. Iyengar, J. Tomasi, M. Cossi, N. Rega, N. J. Millam, M. Klene, J. E. Knox, J. B. Cross, V. Bakken, C. Adamo, J. Jaramillo, R. Gomperts, R. E. Stratmann, O. Yazyev, A. J. Austin, R. Cammi, C. Pomelli, J. W. Ochterski, R. L. Martin, K. Morokuma, V. G. Zakrzewski, G. A. Voth, P. Salvador, J. J. Dannenberg, S. Dapprich, A. D. Daniels, Ö. Farkas, J. B. Foresman, J. V. Ortiz, J. Cioslowski and D. J. Fox, GAUSSIAN 09 (Revision A.1), Gaussian, Inc., Wallingford CT, **2009**.
[76] C. Adamo, V. Barone, *J. Chem. Phys.* **1999**, *110*, 6158–6170.
[77] D. Andrae, U. Haeussermann, M. Dolg, H. Stoll, H. Preuss, *Theor. Chim. Acta* **1990**, *77*, 123–141.
[78] A. Schafer, H. Horn, R. Ahlrichs, *J. Chem. Phys.* **1992**, *97*, 2571–2577.
[79] D. E. Woon, T. H. Dunning Jr., *J. Chem. Phys.* **1994**, *100*, 2975–2988.
[80] T. Lu, F. Chen, *J. Comput. Chem.* **2012**, *33*, 580–592.
[81] W. Humphrey, A. Dalke, K. Schulten, *J. Mol. Graphics* **1996**, *14(27–28)*, 33–38.

Manuscript received: August 4, 2023
Revised manuscript received: November 6, 2023
Accepted manuscript online: November 7, 2023
Version of record online: ■■, ■■

RESEARCH ARTICLE

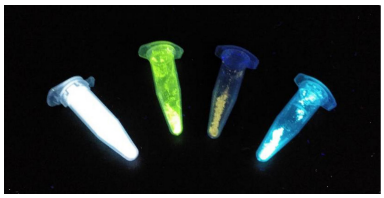

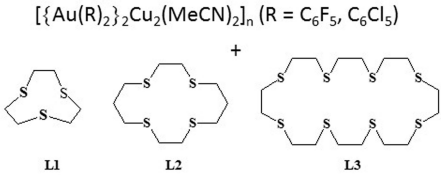

Dr. R. Donamaría, Prof. V. Lippolis, Prof. J. M. López-de-Luzuriaga*, Prof. M. Monge, Prof. M. E. Olmos**

1 – 15

Heteronuclear Gold(I)-Copper(I) Complexes with Thia- and Mixed Thia-Aza Macrocyclic Ligands: Synthesis, Structures and Optical Properties

Heterometallic polynuclear complexes $[\{Au(R)_2\}_2Cu_2(MeCN)_2]_n$ ($R = C_6F_5$, C_6Cl_5) were reacted in THF solution with thioether crowns ligands featuring a different number of S-donor atoms and ring size cavity, and with the quinoline functionalized pendant arm derivatives of tetradentate 12-membered N/S mixed-donor macrocycles. With the latter only ionic compounds of general formula [Cu(**L**)][Au(R)$_2$] (**L** = macrocyclic ligand) were isolated and structurally characterized and none of them featured an Au···Cu metallophilic interaction. The optical properties of all complexes were studied experimentally and theoretically *via* TD-DFT calculations.